Burns & Trauma, 2021, 9, tkab003
doi: 10.1093/burnst/tkab003
Research Article

Research Article

Exosomes of adult human fibroblasts cultured on 3D silk fibroin nonwovens intensely stimulate neoangiogenesis

Peng Hu[1,2,†], Anna Chiarini[1,†,*], Jun Wu[1,3], Giuliano Freddi[4], Kaiyu Nie[2], Ubaldo Armato[1,3] and Ilaria Dal Prà[1,3,†,*]

[1]Human Histology & Embryology Section, Department of Surgery, Dentistry, Paediatrics & Gynaecology, University of Verona Medical School, Strada Le Grazie 8, I-37134, Verona, Venetia, Italy, [2]Department of Burns & Plastic Surgery, The Affiliated Hospital of ZunYi Medical University, 149 Dalian Road, ZunYi City, 563003 Guizhou Province, China, [3]Department of Burns and Plastic Surgery, Second People's Hospital, University of Shenzhen, 3002 Sungang West Road, Futian District, Shenzhen, 518000, Guangdong Province, China, and [4]Silk Biomaterials S.r.l., Via Cavour 2, I-22074, Lomazzo, Lombardy, Italy

*Correspondence. Ilaria Dal Prà, E-mail: ilaria.dalpra@univr.it; Anna Chiarini, E-mail: anna.chiarini@univr.it

[†]These authors equally contributed to the work

Received 12 November 2020; Revised 16 December 2020; Editorial decision 2 February 2021

Abstract

Background: *Bombyx mori* silk fibroin is a biomacromolecule that allows the assembly of scaffolds for tissue engineering and regeneration purposes due to its cellular adhesiveness, high biocompatibility and low immunogenicity. Earlier work showed that two types of 3D silk fibroin nonwovens (3D-SFnws) implanted into mouse subcutaneous tissue were promptly vascularized via undefined molecular mechanisms. The present study used nontumorigenic adult human dermal fibroblasts (HDFs) adhering to a third type of 3D-SFnws to assess whether HDFs release exosomes whose contents promote neoangiogenesis.

Methods: Electron microscopy imaging and physical tests defined the features of the novel carded/hydroentangled 3D-SFnws. HDFs were cultured on 3D-SFnws and polystyrene plates in an exosome-depleted medium. DNA amounts and D-glucose consumption revealed the growth and metabolic activities of HDFs on 3D-SFnws. CD9-expressing total exosome fractions were from conditioned media of 3D-SFnws and 2D polystyrene plates HDF cultures. Angiogenic growth factors (AGFs) in equal amounts of the two groups of exosomal proteins were analysed via double-antibody arrays. A tube formation assay using human dermal microvascular endothelial cells (HDMVECs) was used to evaluate the exosomes' angiogenic power.

Results: The novel features of the 3D-SFnws met the biomechanical requirements typical of human soft tissues. By experimental day 15, 3D-SFnws-adhering HDFs had increased 4.5-fold in numbers and metabolized 5.4-fold more D-glucose than at day 3 *in vitro*. Compared to polystyrene-stuck HDFs, exosomes from 3D-SFnws-adhering HDFs carried significantly higher amounts of AGFs, such as interleukin (IL)-1α, IL-4 and IL-8; angiopoietin-1 and angiopoietin-2; angiopoietin-1 receptor (or Tie-2); growth-regulated oncogene (GRO)-α, GRO-β and GRO-γ; matrix metalloproteinase-1; tissue inhibitor metalloproteinase-1; and urokinase-type plasminogen activator surface receptor, but lesser amounts of anti-angiogenic tissue inhibitor metalloproteinase-2 and pro-inflammatory

monocyte chemoattractant protein-1. At concentrations from 0.62 to 10 μg/ml, the exosomes from 3D-SFnws-cultured HDFs proved their angiogenic power by inducing HDMVECs to form significant amounts of tubes *in vitro*.

Conclusions: The structural and mechanical properties of carded/hydroentangled 3D-SFnws proved their suitability for tissue engineering and regeneration applications. Consistent with our hypothesis, 3D-SFnws-adhering HDFs released exosomes carrying several AGFs that induced HDMVECs to promptly assemble vascular tubes *in vitro*. Hence, we posit that once implanted *in vivo*, the 3D-SFnws/HDFs interactions could promote the vascularization and repair of extended skin wounds due to burns or other noxious agents in human and veterinary clinical settings.

Highlights

- This work reports, for the first time, the structural and mechanical features of novel carded and hydroentangled 3D-SFnws fitting the requirements for human soft tissue engineering/regeneration.
- Adult HDFs adhering to such carded/hydroentangled 3D-SFnws continued growing, metabolizing D-glucose and extracellularly releasing exosomes for at least 15 days *in vitro*.
- The exosomes released from 3D-SFnws-adhering HDFs carried high amounts of 10 different angiogenic/growth factors that powerfully induced human dermal microvascular endothelial cells to rapidly form tubes *in vitro*.
- These findings suggest that by interacting with local HDFs, grafted 3D-SFnws would crucially advance the vascularization and healing of extended and deep skin wounds caused by burns or other noxious agents.

Key words: Silk fibroin, Nonwovens, Dermis, Fibroblast, Human endothelial cell, Exosome, Cytokine, Chemokine, Angiogenesis, Regeneration, Tissue engineering

Background

Silk fibroin (SF) is a fibrous biomacromolecule of natural origin [1]. Native *Bombyx mori* SF microfibers are used not only to weave cloths but also to produce biomaterial scaffolds [2]. The best balance between biocompatibility, mechanical properties and biodegradability makes SF an excellent substrate for scaffolds suitable for guided tissue engineering and regenerative medicine applications [3]. Moreover, SF allows for a highly versatile scaffold design, thanks to the many processing options that one can implement [4]. Besides native SF microfibers, several regenerated SF materials, such as films, hydrogels, porous sheets, electrospun mats and nanofibers, have attracted intense interest as implantable medical devices. The host reaction in terms of tissue–implant interface dynamics, *de novo* vascularization and immune response is crucial for the successful clinical outcome of grafted devices [5]. In recent years, several kinds of SF scaffolds have been preclinically tested *in vitro* and *in vivo* using small and large animal models; some of these devices have reached the clinical trial stages, and a few have entered the market [6].

In the context of skin tissue engineering and regeneration we are interested in SF-based scaffolds structured as nonwovens [7–10]. In earlier studies, we investigated the *in vitro* and *in vivo* biological responses evoked by two novel types of 3D SF-based nonwovens (3D-SFnws) made of randomly oriented native SF microfibers either glued with formic acid (FA) or interlaced by combining carding and needling textile technologies [8–10]. Observations lasting for up to 6 months revealed for the first time the results of implanting either of these 3D-SFnws into the subcutaneous layer of C57/BL6 mice. Histological studies showed that the biocompatibility of 3D-SFnws was quite good as they only elicited a mild foreign body response with no sign of fibrosis or encapsulation. This is most interesting, since the first week after grafting abundant proliferating capillaries with an accompaniment of fibroblasts migrated first along the microfibres of both types of 3D-SFnws prior to colonizing the interposed voids. The upshot was the guided generation of a well-vascularized reticular connective tissue, which incorporated the SF microfibers and filled the intercalated spaces [8, 10]. However, the biological mechanism underlying the effective vascularization of the *in vivo* newly formed reticular connective tissues remained unknown.

Notoriously, human dermal fibroblasts (HDFs) release compounds such as growth factors, enzymes, cytokines and chemokines. These are cell-to-cell signalling polypeptides or small soluble proteins that play relevant roles in angiogenesis, cell growth, cell differentiation, inflammation, innate immunity and apoptosis [11–16]. Cellular mechanisms other than the classical exocytosis partake in such signalling, including the discharge of variously sized membranous extracellular vesicles. The latter include nanoscale (diameter, 30–120 nm) vesicles, which are named exosomes, carrying specific provisions of proteins, lipids, DNA and RNAs [17–19]. Exosomes are advantageous because they allow the concentration and delivery of cytokines, chemokines, angiogenic growth factors (AGFs) and other agents to adjacent or distant cells via the extracellular matrix (ECM), blood, saliva, urine and cerebrospinal fluid. This can happen because exosomes protect their cargoes from breakdown by environmental degradation mechanisms. The exosomes elicit specific biological responses after endocytosis or by interacting with the plasma membrane

surface of cells, from which the cellular receptors for most cytokines, chemokines and AGFs stick out. Thus, exosomal cargoes can effectively modulate intracellular signalling pathways, homeostatic mechanisms, antigen presentation, angiogenesis, coagulation, inflammation and apoptosis [20–23]. Several laboratories have reported that exosomes released from various cell types, such as mesenchymal stem cells and endothelial cells (ECs), promote regeneration of vascular ECs and angiogenesis [24, 25]. Based upon our *in vivo* observations [8, 10], we posited that mouse fibroblasts which had met the implanted 3D-SFnws may have released exosomes carrying a powerful mixture of angiogenic factors. To evaluate this hypothesis and its potential relevance in translational medicine, we devised an experiment using HDFs cultured on a novel 3D-SFnws scaffold to assess the contents and amounts of any AGFs carried by the HDF-released exosomes. We reported here that adult HDFs adhering to the novel 3D-SFnws release exosomes carrying 18 different AGFs in protein form, of which 10 are in amounts much higher than in exosomes supplied by HDFs adhering to 2D polystyrene surfaces. We also showed that the exosomes from 3D-SFnws-adhering HDFs exert a powerful angiogenic effect on human dermal microvascular endothelial cells (HDMVECs) *in vitro*. These findings support the view that such novel 3D-SFnws scaffolds, once implanted in burn or trauma wound beds, would promote their own vascularization and cellular colonization, thus successfully advancing tissue engineering and regeneration and healing.

Methods

Production of the carded/hydroentangled 3D-SFnws

Sericin-deprived (via standard de-gumming) spun silk from comber waste in staple form (average fibre length, 50 ± 7 mm) was the starting material used to produce the 3D-SFnws. This SF material underwent processing in a cotton-type flat carding machine (width, 100 cm). Web formation by carding arranged the fibres in bundles that took a preferential lengthwise orientation, i.e. an alignment in the longitudinal direction of the nonwoven web (henceforth indicated as machine direction (MD)). Next, the carded web received on both its surfaces a mechanical hydroentanglement that created several bonding points on it [26].

Scanning electron microscopy (SEM)

To be morphologically analysed, 3D-SFnws were sputter coated with Au/Pd under a reduced-argon atmosphere in a Desk IV Coating System (Denton Vacuum, USA) and observed in a Zeiss EVO MA10 scanning electron microscope under the following conditions: 10 kV acceleration voltage, 100 mA beam current and 15 mm working distance.

Attenuated total reflectance Fourier transform infrared spectroscopy

An ALPHA Fourier transform infrared spectrometer (Bruker, Italy) equipped with an attenuated total reflectance platinum diamond accessory served to analyse the samples by collecting 65 scans at a 4 cm^{-1} resolution in the infrared 4000–400 cm^{-1} wavenumber range. Spectra were corrected with a linear baseline and normalized to the CH_2 bending peak at about 1445 cm^{-1}, a peak notoriously insensitive to the molecular conformation of SF.

Differential scanning calorimetry

A calorimeter (DSC 3500 Sirius, Netzsch, Germany) determined the thermal properties of the SF nonwovens. Samples (3–5 mg) were sealed in aluminium pans and subjected to a heating cycle from 50°C to 400°C, at a heating rate of 10°C/min, under a sweeping N_2 atmosphere (flow rate, 20 ml/min).

Physical properties and tensile measurements

Thickness, mass per unit area and density per unit volume of 3D-SFnws were measured according to the UNI EN ISO 5084:1998 and UNI EN 12127:1999 standard methods. The values of stress, strain and Young's modulus of 3D-SFnws in both the MD and the transversal direction (TD) were calculated from the load elongation curves recorded under wet conditions. Before analysis, an overnight soaking in water of test specimens 100 mm long and 10 mm wide achieved full hydration. After removing the excess water with blotting paper, specimens were clamped on the jaws of the tensile testing machine (Instron 3345, Instron, Italy) equipped with a 500 N load cell. The gauge length was 50 mm. Measurements were conducted at a temperature of 20°C with a relative humidity of 65%. After applying a preload of 0.5 N the test was run at 50 mm/min crossbar rate. Six specimens of 3D-SFnws were analysed for either direction. The thickness of 3D-SFnws, measured according to ISO 5084:1996, was 0.55 ± 0.03 mm. This value served to calculate the stress from experimental load values.

Preparation of 3D-SFnws for *in vitro* cell cultures

After a thorough washing in phoshate buffer saline (PBS), 3D-SFnws samples were transversally cut into rectangular pieces measuring 66×23 mm, sealed in pouches and sterilized at 55°C for 3 hours via exposure to an ethylene oxide/CO_2 (10/90 v/v) mixture under a pressure of 42 psi in a vacuum oven. Next, specimens were kept for 24 hours in an aeration room followed by an 8-hour degassing at 50°C in a vacuum oven. Prior to use, the sterilized 3D-SFnws were systematically tested by checking for the absence of morphological changes and the maintenance of mechanical properties. Finally, the sterilized 3D-SFnws samples were aseptically transferred to 4-well, multi-dish lidded, sterile, polystyrene culture plates (Cat. No. 176597, Nalge Nunc International, USA). Sterilized steel rods flattened the edges of the 3D-SFnws samples at the bottom of the plates.

Cells

HDFs were bought from ScienCell Research Laboratories (USA). The supplier company guaranteed, via Cell

Applications (USA), that the HDFs expressed fibronectin and were negative for immune deficiency virus, hepatitis B virus, hepatitis C virus, mycoplasma, bacteria, yeasts and fungi. The standard culture medium for the HDFs was Dulbecco's minimum essential medium (DMEM) (89% v/v; Life Technologies Italia, Italy) supplemented with heat-inactivated (at 56°C for 30 minutes) foetal bovine serum (FBS) (10% v/v; Life Technologies Italia) and penicillin–streptomycin solution (1% v/v; Lonza, Italy).

HDMVECs isolated from adult skin capillaries were sourced from Cell Applications (USA). The seller pledged that such cells were free from bacteria, yeasts, fungi and mycoplasma, and that they expressed the factor VIII-related antigen. HDMVECs were grown in endothelial cell growth basal medium (PromoCell, Germany) supplemented with 10% v/v inactivated FBS; for the experiments, the standard FBS was changed to bovine exosome-depleted FBS.

Preparation of cell culture medium devoid of bovine exosomes

To ensure that the exosomes under study came solely from the HDFs, with no contamination from FBS-carried exosomes, the experimental growth medium was fortified with a 2.5% v/v exosome-depleted FBS. To achieve this, prior to being added to the cell culture medium the heat-inactivated (at 56°C for 30 minutes) FBS underwent 2 centrifugations at 100,000 × *g* for 120 min in an Optima TLX ultracentrifuge using the minirotor type TLA 100.3 (Beckman, USA) [27].

Intravital HDF staining

Prior to their experimental use, 3rd or 4th passage HDFs were counted using a handheld automated cell counter (Scepter, Merck, Germany) according to the manufacturer's instructions. To highlight the cells adhering to the 3D-SFnws just prior to seeding, 2×10^6 HDFs were intravitally stained with fluorescent lipophilic membrane dyes (tracers): the red-orange fluorescent 1,1′-Dioctadecyl-3,3,3′,3′-tetramethyl-indocarbocyanine perchlorate (fluorescence excitation λ_{max}, 549 nm; emission λ_{max}, 565 nm) or the green fluorescent 3,3′-Dioctadecyl oxacarbocyanine perchlorate (fluorescence excitation λ_{max}, 484 nm; emission λ_{max}, 590 nm) (both from Thermo Fisher Scientific, Italy). These dyes were dissolved in dimethyl-sulfoxide, DMSO and used to intravitally stain HDFs according to the manufacturer's instructions. For each experiment, 4 equal aliquots (5×10^5 each) of pre-stained HDFs were carefully seeded onto four 3D-SFnws scaffolds placed inside separate Petri dishes (diameter, 10 cm; Thermo Fisher Scientific, Italy). For comparative purposes, equal aliquots (5×10^5 cells each) of pre-stained HDFs were seeded in parallel onto 4 identical polystyrene Petri dishes. The cell cultures of both groups were incubated for 15 days at 37°C in a 95% v/v air, 5% v/v CO_2 atmosphere. HDFs were regularly seen under an inverted fluorescence microscope (IM35, Zeiss, Germany) fitted with proper excitation and emission filters. All the later procedural steps were the same for the control group and the experimental group.

PicoGreen DNA quantification

To estimate the cell proliferation onto 3D-SFnws, DNA cellular contents were assessed by the Quant-iT PicoGreen dsDNA Kit (Thermo Fisher Scientific). Three specimens of HDFs cultured on 3D-SFnws were assessed at experimental days 3 and 15. After washing the cells in PBS, 8 ml of deionized water was added to the wells to detach and lyse the cells. Repeated vortexing and two freezing–thawing cycles improved cell lysis. DNA amounts were then fluorometrically measured at excitation λ 480 nm and emission λ 520 nm. A standard double strand DNA curve of known concentrations was used to calibrate the fluorescence intensities.

Assay of D-glucose consumption

Cell D-glucose cumulative consumption was assessed in conditioned growth media samples from HDFs cultured on 3D-SFnws by a glucose oxidase assay using the Amplex Red Glucose/Glucose Oxidase Assay Kit (Thermo Fisher Scientific, Italy). Glucose oxidase reacted with D-glucose to form D-gluconolactone and hydrogen peroxide via horseradish peroxidase. Hydrogen peroxide reacted with the Amplex Red reagent in a 1:1 stoichiometric ratio to generate the red-fluorescent product resorufin, the intensity of which was recorded fluorometrically at excitation and emission wavelengths of 560 and 590 nm, respectively.

Isolation and quantification of exosomes

HDF-conditioned media of both experimental and control groups were collected at 72-hour intervals and centrifuged at 2000 × *g* for 30 minutes at 4°C to remove cells and debris. The resulting supernatants were stored at −80°C for later analysis. After thawing, the supernatants of either group were pooled and the corresponding total exosomal fractions were extracted using the Total Exosome Isolation Reagent for cell culture media (No. 4478359, Thermo Fisher-Invitrogen, USA) following the manufacturer's protocol with slight modifications. Briefly, the supernatants were centrifuged for 30 minutes at 15,000 × *g*, mixed with the proprietary reagent, incubated overnight at 4°C and then centrifuged again for 90 minutes at 10,000 × *g* at 4°C. The exosome fractions were contained in the final pellets. This procedure has been compared with others and validated [28]. The total proteins of the exosome fractions were quantified using Bradford's method. The marker-based assessments of exosomal preparations were completed using an enzyme-linked immunosorbent assay (ELISA) kit that detects the CD9 marker (ExoTEST™, HansaBio Med, Estonia). Notably, CD9 is a tetraspanin protein intensely expressed by fibroblasts and a typical marker present at the membrane surface of HDF-released exosomes [29]. Therefore, equal amounts of exosomal proteins from the experimental and control groups were used in parallel for later processing steps.

Identification and quantitation of exosome-carried AGFs

The several exosome-carried AGFs were identified and quantified with the Human Angiogenesis Antibody Array C1000 (RayBiotech, USA) according to the manufacturer's protocols. Briefly, equal amounts of exosomal proteins of the control and experimental group were diluted in 2.0 ml PBS and then incubated with the antibody arrays, which had been pretreated for 30 minutes with Odissey blocking buffer (LI-COR, USA). After an overnight incubation at 4°C and a thorough washing, the array membranes were incubated for 2 hours with 1.0 ml of a mix of array-specific biotin-conjugated primary antibodies, diluted 1:250 in Odissey blocking buffer. Finally, the membranes were incubated at room temperature for 1 hour with 2.0 ml of DyLight800-conjugated streptavidin (KPL, USA), diluted 1:7500 in Odissey blocking buffer. The positive signals of the several AGFs were acquired with an Odissey scanner (LI-COR, USA) and their densitometric values quantified by using the Image Studio software package (version 5.2, LI-COR, USA). Each array's positive signal intensity values were normalized via comparisons to correlated positive controls. The results from 3 independent experiments were averaged and expressed as mean values ± standard deviations (SDs). This technology provides several advantages: (1) it allows the performance of high-content screening using about the same sample volume as required by traditional ELISAs; (2) it improves the chances of discovering key factors while maintaining an ELISA-like sensitivity; (3) it has a wider detection range, i.e. 10,000-fold, than typical ELISAs (i.e. 100–1000-fold); and (4) it has a lower inter-array coefficient of variation of spot signal intensities (∼5–10%) than typical ELISAs (∼10–15%).

Endothelial tube formation assay

The pro-angiogenic properties of exosomes released from HDFs grown on 3D-SFnws scaffolds were assessed using HDMVECs and the PromoKine Angiogenesis Assay Kit (Cat. No. PK-CA577-K905, PromoCell, Germany) according to the manufacturer's instructions. Briefly, HDMVECs were grown at 37°C in air with CO_2 5% v/v until reaching about 90% confluency in endothelial cell growth basal medium (Cat. No C-22210, PromoCell, Germany) with added supplement mix (Cat. No C-39215, PromoCell, Germany). Next, HDMVECs were harvested using trypsin 0.025% v/v and resuspended in endothelial cell growth basal medium fortified with 2.5% v/v exosome-depleted FBS. Then, an aliquot (50 µL) of ECM solution was added to each well of a 96-well sterile cell culture plate kept on ice that was thereafter incubated at 37°C to form a gel. After that, 20×10^3 HDMVECs suspended in 100 µL culture medium were mixed with different concentrations (i.e. 0.625, 1.25, 2.5, 5.0 and 10.0 µg/ml) of exosomes from 3D-SFnws-adhering HDFs or with no exosomes (controls on polystyrene ± ECM gel) and directly added to each well. Finally, the plates were incubated at 37°C in air with CO_2 5% v/v for 5 hours. HDMVECs were checked and photographed at ×400 magnification under an IM35 microscope with an Olympus DP10 digital camera (Olympus, Japan). The mean tube lengths in µm per microscopic field at ×100 magnification were quantified via morphometric methods [30]. Triplicate results were averaged and expressed as the means ± SDs.

Statistical analysis

Data were expressed as mean values ± SDs. Descriptive statistical analyses were conducted using the Analyse-it software package (Analyse-it, UK). A Shapiro–Wilk test showed that the data groups had normal distributions. A one-sided Student's *t*-test served to assess the level of statistical significance between differences of data means from HDFs cultured on 3D-SFnws versus HDFs cultured on polystyrene. A one-way analysis of variance with a *post hoc* Tukey's test served for multiple comparisons of the results from endothelial tube formation assays. The statistical significance level was set at $p < 0.05$.

Results

Morphological, physical, chemical, and mechanical features of the novel 3D-SFnws

Fibres of a 50 ± 7 mm length made the carded/hydroentangled 3D-SFnws, which were 520 µm thick, weighed 58 g/m^2 and had a density of 105 g/m^3.

Scanning electron microscopy observations revealed the surface morphology and fine structure of these 3D-SFnws (Figure 1a, b, c). The SF microfibres formed a network limiting a high number of intercommunicating voids. At first sight, the pictures are similar to those other two previously published proper types of SF-based nonwovens [8, 10]. However, at low magnification (Figure 1a) it becomes manifest that the preferential orientation of the SF microfibers corresponds to the direction (or MD) of the web carding. Figure 1b shows the details of a bonding point, where the SF fibres were forced to become twisted together by the mechanical action of the water (hydroentangling). The 3D-SFnws microfibres have a diameter ranging from 7 to 14 µm and no film-like or other structure linking them together. In fact, the void spaces interspersed between the microfibers are clear. In addition, Figure 1c documents the clean and smooth surface of the 3D-SFnws microfibres, proving the perfect sericin removal.

The chemical and physical characterization of the 3D-SFnws was performed via infrared spectroscopy (attenuated total reflectance Fourier transform infrared), differential scanning calorimetry and stress/strain application.

Figure 1d showed the typical attenuated total reflectance Fourier transform infrared spectrum of the 3D-SFnws samples from the 2000 to 800 cm^{-1} wavenumber range. Such a spectral range is the fingerprint of SF, as it shows several absorption bands strongly affected by its physical and chemical structure [31, 32]. The bands at 1618 cm^{-1} (amide I), 1510 cm^{-1} (amide II) and 1227 cm^{-1} (amide III) are typically SF conformation sensitive as they arise from different vibrational modes of the peptide bond. The weak bands at 975 cm^{-1} and 997 cm^{-1} are specific to

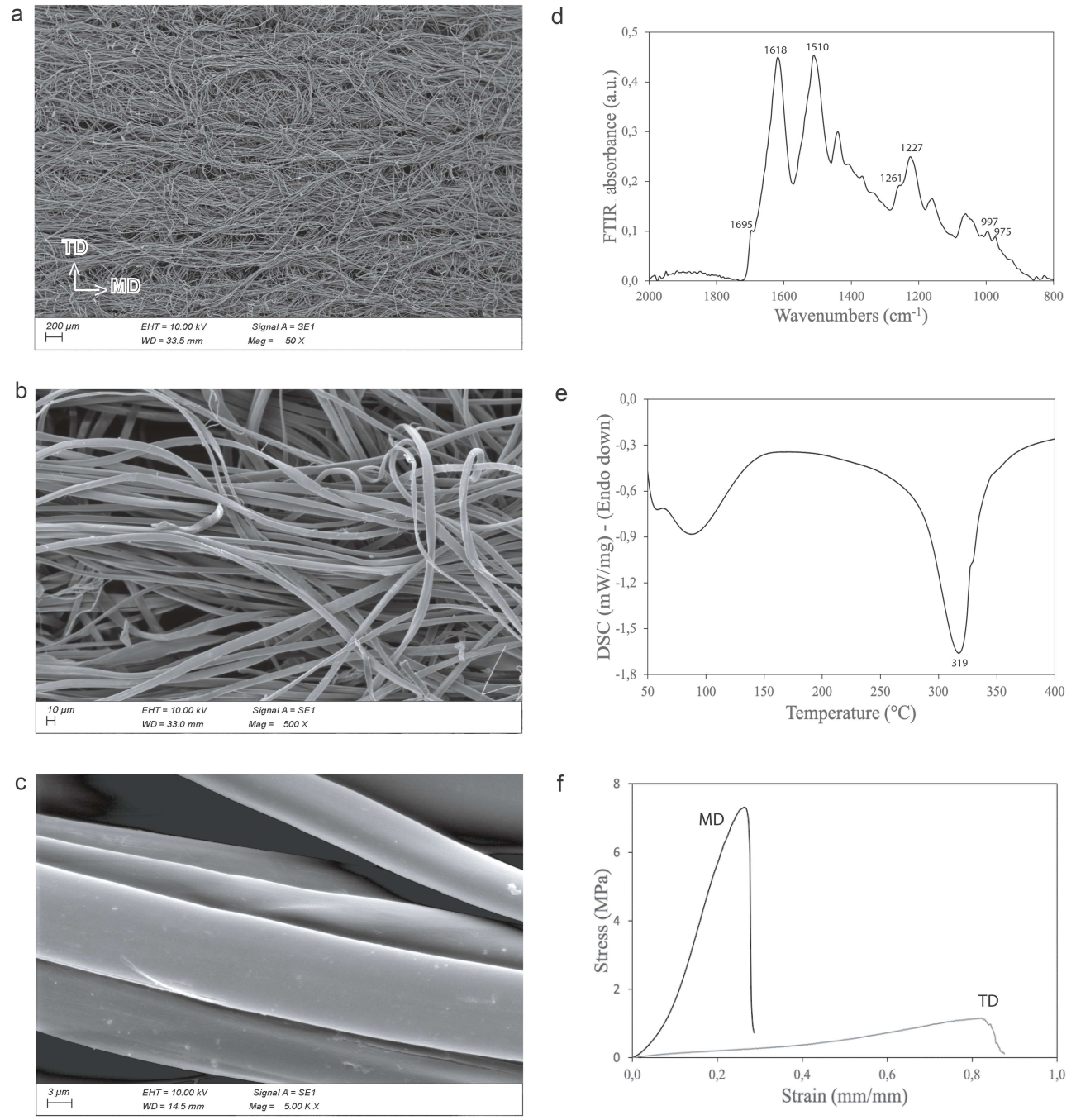

Figure 1. Silk fibroin (SF) microfibers and their nodes in the novel 3D SF nonwovens (3D-SFnws) produced via the carding/hydroentanglement technology. Scanning electron microscopy at low (×50) **(a)**, medium (×500) **(b)** and high (×5000) **(c)** magnifications. In **(a)**, the white arrows show the machine direction (MD) and transversal (TD) direction, respectively, of the 3D-SFnws fabrics. **(d)** Attenuated total reflectance Fourier transform infrared spectroscopy (FTIR) spectrum of the 3D-SFnws in the 2000 cm^{-1} to 800 cm^{-1} wavenumber range. The bands of Amide I at 1618 cm^{-1}, Amide II at 1510 cm^{-1} and Amide III at 1227 cm^{-1}, with a shoulder at about 1261 cm^{-1}, are typical of the β-sheet molecular conformation of crystalline and oriented SF fibres. **(e)** Differential scanning calorimetry (DSC) thermogram of the novel 3D-SFnws. The strong melting/degradation peak at 319°C characterizes the SF fibres with a high degree of molecular order and crystallinity. **(f)** Representative stress/strain curves of the novel 3D-SFnws in the MD and the TD under wet conditions. Electron high tension, EHT; working distance, WD; magnification, Mag.

the repetitive Gly-Ala and Gly-Gly sequences of the SF chain, respectively. Altogether, these bands give back the image of a native silk material with a highly stable β-sheet molecular conformation typical of the crystalline and oriented SF fibres.

Figure 1e shows the differential scanning calorimetry thermogram of the 3D-SFnws. It demonstrates a strong melting/degradation peak at 319°C that again is characteristic of the SF fibres endowed with a high degree of molecular order and crystallinity [32].

Table 1. Tensile properties of 3D silk fibroin nonwovens

	Carded-hydroentangled		Carded-needled [10]	FA-crosslinked [8, 9]
	MD	TD	MD/TD	MD/TD
Stress (MPa)	6.91 ± 0.3	1.8 ± 0.1	2.5 ± 0.6	4.9 ± 0.6
Strain (%)	26 ± 2.0	0.80 ± 0.1	49.4 ± 5.9	21.4 ± 2.5
Young's modulus (MPa)	38.4 ± 1.6	1.9 ± 0.3	8.0 ± 1.6	34.4 ± 2.7

Carded-hydroentangled nonwovens are stronger (value of stress is significantly higher than the other 2), less elastic than carded-needled nonwovens (value of strain is about one-half) but more elastic than FA-crosslinked nonwovens. The Young's modulus estimates the degree of stiffness, which is the resistance to deform following the application of a small load. Carded-hydroentangled nonwovens are as stiff as FA-crosslinked nonwovens in the MD but much more pliable and compliant than the other 2 nonwovens in the TD. The carded-needled and FA-crosslinked nonwovens have identical mechanical properties in the 2 directions. Data are mean value ± standard deviation. *FA* formic acid, *MD* machine direction, *TD* transversal direction

Moreover, Figure 1f shows representative stress/strain curves of the 3D-SFnws in the MD and the TD [32]. The corresponding tensile measurements reported in Table 1 confirm the mechanical robustness of the 3D-SFnws. As expected, a clear mechanical anisotropy along the two axes characterizes these scaffolds. The latter are stronger and stiffer in the MD due to the preferential alignment of the lengthy SF fibre bundles caused by the carding process. The values of stress, strain and Young's modulus in the MD are equal or even better than those of the nonwoven silk matrices we previously reported [8, 10]. On the other hand, the present 3D-SFnws are much more pliable in the TD than the earlier nonwoven silk matrices [8, 10] (Table 1). Altogether, these properties reveal that the current material is highly performing in terms of meeting the biomechanical requirements typical of human soft tissue [33]. Translating into biological terms, according to Wang *et al*. [34] and Thurber *et al*. [3], these properties mean that once implanted *in vivo* the 3D-SFnws under study may have a medium- to long-term degradation profile, hence providing an effective biomechanical support to the *de novo* engineering of the intended biological structure.

Growth and metabolism of HDFs grown on 3D-SFnws

After careful seeding, 70–80% of the intravitally stained HDFs attached within 3 hours onto the 3D-SFnws. Microscopy observations confirmed the HDFs numerical increase with time (Figure 2a, b, c, d). The growth of the adhering cells between experimental days 3 and 15 was mirrored by a 4.5-fold increase in the double strand DNA amount associated to the 3D-SFnws (Figure 2e). Biochemical assays showed that the cumulative D-Glucose consumption by the HDFs adhering to 3D-SFnws increased 5.4-fold between experimental days 3 and 15 in culture, i.e. values paralleling the HDF numerical increases (Figure 2f). On the other hand, polystyrene-adhering HDFs started growing after the first 24 hours and kept doing so until they reached confluence by the 14th day (not shown).

AGF amounts released via exosomes from HDFs grown on 3D-SFnws versus polystyrene

Specific membrane-based double-antibody arrays allowed us to identify and quantify the AGFs carried by equal amounts of the pooled exosomes released from HDFs grown on 3D-SFnws and on polystyrene [35].

Typical developed array membranes—a couple of membranes for each experimental group to cover the whole series of compounds evaluated—are comparatively shown in Figure 3a, b, c, d. The results of the arrays showed that 18 out of the 43 potentially discoverable AGFs were carried by the HDF-released exosomes of both experimental groups (Figure 3a, b, c, d) (Table S1). The quantitative analysis and statistical comparison of corresponding spots showed that the amounts of 10 out of the 18 exosome-carried AGFs from the 3D-SFnws-grown group were significantly higher and 2 others significantly lower than in the exosomes from the polystyrene-grown group ($p < 0.05$) (Figure 4). The highest percent increases in the 3D-SFnws versus the polystyrene group were those of tissue inhibitor of metalloproteinase-1 (TIMP)-1 (+187%), interleukin (IL)-8 (+117%) and growth-regulated oncogene (GRO)-α, GRO-β and GRO-γ chemokines (+63%). Lesser but still significant increases in the 3D-SFnws group versus the polystyrene group were those of urokinase-type plasminogen activator surface receptor (uPAR) (+53%), angiopoietin (ANGPT)-1 (+49%), IL-1α (+48%), ANGPT-2 (+46%) and IL-4 (+40%). Still smaller percent increases were those of matrix metalloproteinase (MMP)-1 (+33.5%) and ANGPT-1-R receptor (or Tie-2; +25%). The remaining 2 factors, tissue inhibitor of metalloproteinase-2 (TIMP-2) (−25%) and monocyte chemoattractant protein-1 (MCP-1) (−44%), were significantly less abundant in the exosomes from the 3D-SFnws group than in those from the polystyrene group (Figure 4).

Conversely, the exosomal amounts of the remaining 6 compounds identified—plasminogen/angiostatin, IL-1β, MMP-9, fibroblast growth factor (FGF)-2, IL-6 and vascular endothelial growth factor (VEGF)-D—did not significantly ($p > 0.05$) differ between the 3D-SFnws group and the polystyrene group (Table 2).

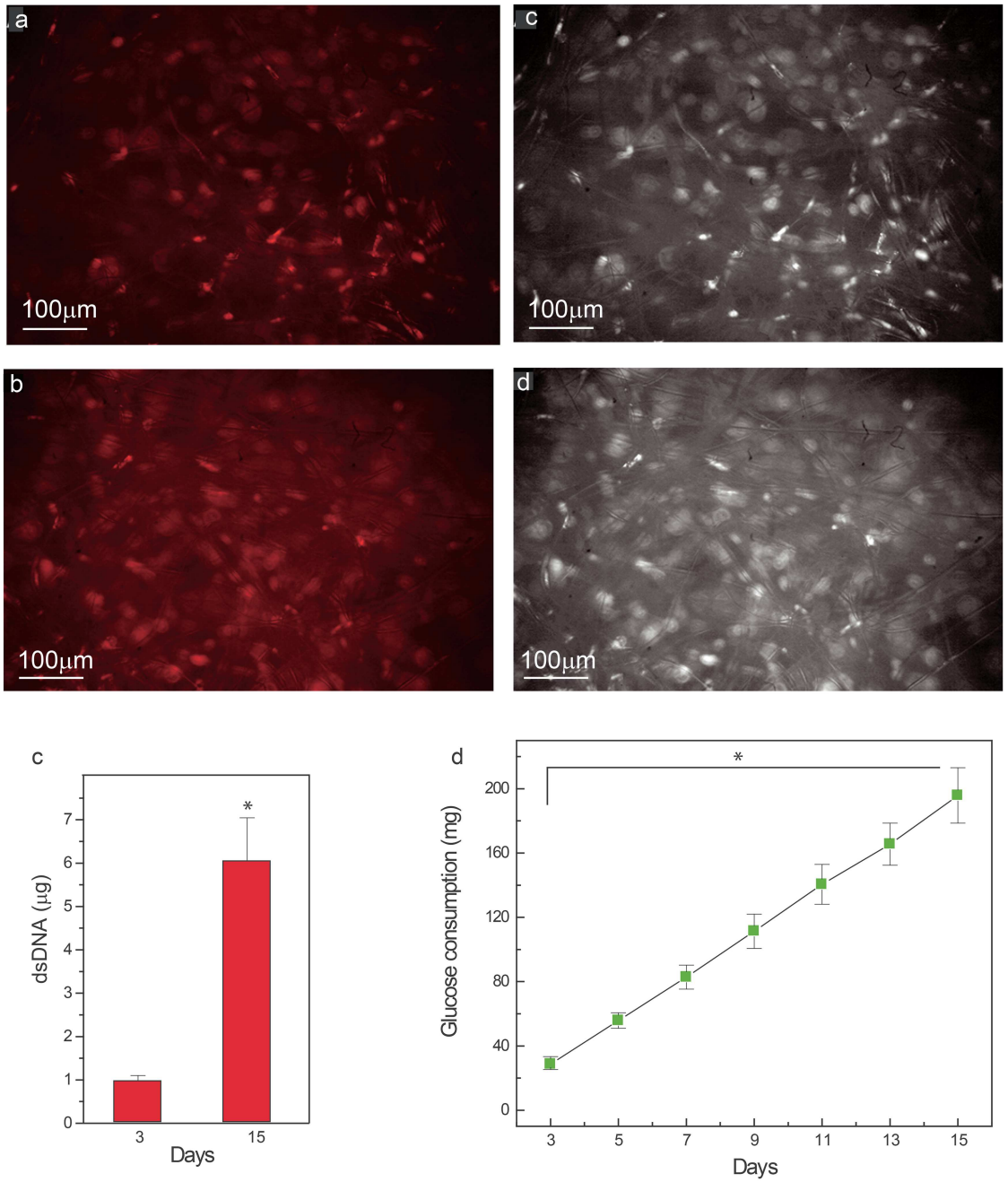

Figure 2. The morphology, growth and metabolic activity of human dermal fibroblasts (HDFs) that had adhered to and colonized the 3D silk fibroin nonwovens (3D-SFnws). **(a, b)** Intravitally 1,1′-Dioctadecyl-3,3,3′,3′-tetramethyl-indocarbocyanine perchlorate pre-stained HDFs on 3D-SFnws seen under a fluorescence inverted microscope emit a red fluorescence at λ 565 nm due to the lipophilic stain incorporated by their cellular membranes. The 3D-SFnws microfibers do not emit any interfering fluorescence at λ 565 nm and hence are hardly detectable. Obviously, most of the visible cells are out of focus since they are attached to a 3D scaffold. However, the cell numbers are noticeably higher at 5 days **(b)** than at 2 days after plating **(a)**. **(c, d)** These are the same pictures as in **(a)** and **(b)**, respectively, as they appear after digitally removing the red colour. Under these conditions it is possible to detect very thin black stripes at certain sites running in parallel, which correspond to the SF microfibers of the 3D-SFnws. Some of these stripes run over and cut the images of the underlying cells. Original magnification in **(a)** and **(b)**, ×40. **(e)** HDFs attached to 3D-SFnws significantly increase their numbers during 15 days of staying *in vitro* as shown by the 4.5-fold increase in number of the cells adhering to the scaffolds between day 3 and day 15. Double strand (ds) DNA amounts were assayed as detailed in the Methods. Bars are mean value ± standard deviation (SD) from 3 distinct duplicate determinations at each time point. $^{*}p < 0.001$. **(f)** The cumulative D-Glucose consumption of HDFs cultured on 3D-SFnws. D-Glucose levels of the HDF-conditioned media at each time point were gauged as detailed in the Methods. Each dot represents the mean value ± SD from 3 distinct duplicate determinations. $^{*}p < 0.001$

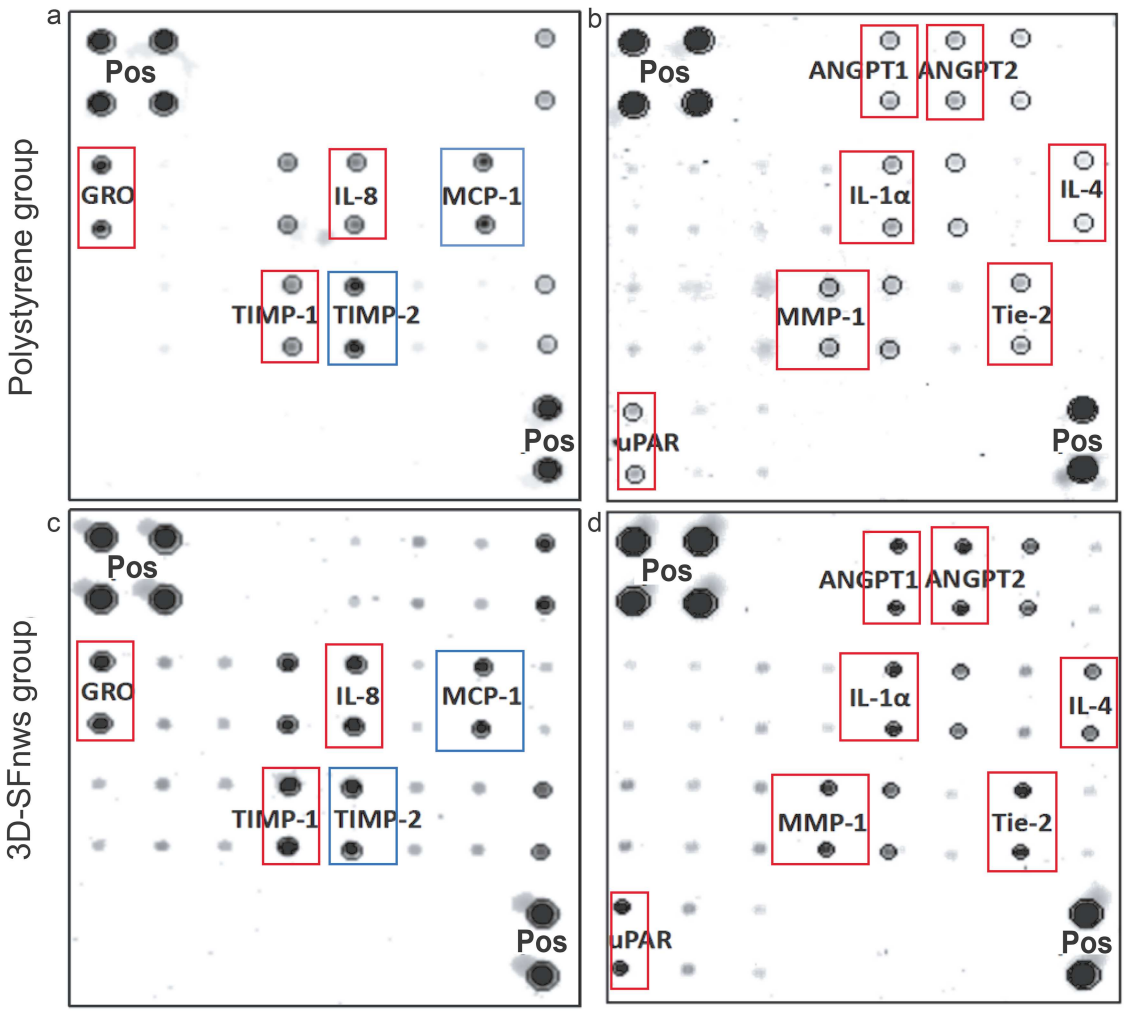

Figure 3. Developed double-antibody array membranes (each array made of 2 different membranes) showing the angiogenic/growth factors (AGFs) carried by the exosomes released from human dermal fibroblasts (HDFs) grown either as conventional monolayers on polystyrene **(a, b)** or on 3D silk fibroin nonwovens (3D-SFnws) **(c, d)**. Equal amounts of exosomes isolated from HDF-conditioned media samples of the 2 experimental groups were used. For technical details consult the Methods section. The red rectangles include the duplicate dots of each of the AGFs whose exosomal amounts were significantly ($p < 0.05$) higher, and the blue rectangles enclose those whose amounts were lower ($p < 0.05$) when comparing the 3D-SFnws group with the polystyrene group. *ANGPT* angiopoietin, *GRO* growth-regulated oncogene, *IL* interleukin, *MCP-1* monocyte chemoattractant protein-1, *MMP-1* matrix metalloprotease-1, *Pos* positive control spots, *TIMP* tissue inhibitor of metalloproteinases, *uPAR* urokinase-like plasminogen activator surface receptor

Table 2. Other angiogenic/growth factors carried by equal amounts of exosomes from either group

AGFs	Polystyrene group	3D-SFnws group	Δ%	*P* value
Plasminogen (Angiostatin)	7. 7 ± 0.72	9.41 ± 0.925	+22.2	0.218
Interleukin-1β	6.94 ± 0.648	8.37 ± 0.81	+20.6	0.240
Matrix metalloprotease-9	8.24 ± 0.803	9.53 ± 0.915	+15.7	0.349
Fibroblast growth factor-2/b	37.8 ± 2.7	43 ± 3.03	+13.8	0.269
Interleukin-6	56.4 ± 5.39	57.3 ± 5.06	+1.8	0.909
Vascular endothelial growth factor-D	27.0 ± 2.87	24.9 ± 2.38	-7.8	0.603

Data are mean value ± standard deviation of the densitometric integral intensity assessments for each factor from 3 independent experiments each with duplicate determinations. Numbers shown are the original values $\times 10^3$

3D-SFnws 3D silk fibroin nonwovens, *AGFs* angiogenic growth factors

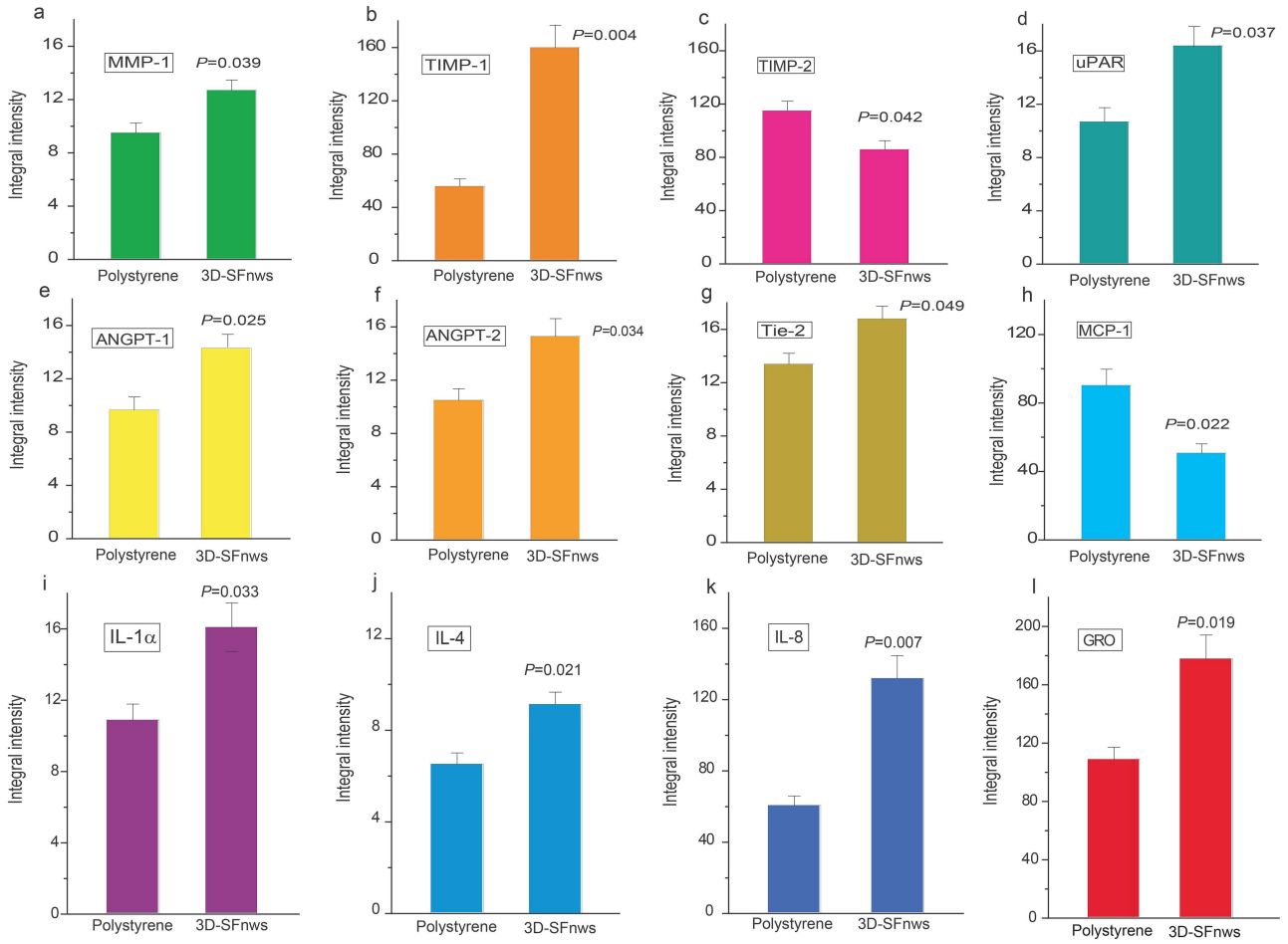

Figure 4. Significantly changed exosomally carried AGFs are here tiered as (1) those affecting pro-angiogenic (MMP-1, TIMP-1, uPAR) and anti-angiogenic (TIMP-2) ECM remodelling (**a–d**); (2) those mainly angiogenic (ANGPT-1, ANGPT-2, Tie-2) and proinflammatory (MCP-1) (**e–h**); and (3) those both angiogenic and mitogenic (IL-1α, IL-4, IL-8, GRO-α, GRO-β and GRO-γ) (**i–l**). In detail, **(a)** MMP-1; **(b)** TIMP-1; **(c)** TIMP-2; **(d)** uPAR; **(e)** ANGPT-1; **(f)** ANGPT-2; **(g)** Tie-2; **(h)** MCP-1; **(i)** IL-1α; **(j)** IL-4; **(k)** IL-8; **(l)** GRO-α, GRO-β and GRO-γ. These factors were assayed as detailed in the caption for Figure 3 on equal amounts of exosomal proteins from either experimental group. The bars are mean value ± standard deviation from 3 distinct experiments, each conducted in duplicate. The corresponding *p* values of the differences between each couple of bars are also shown. *ANGPT* angiopoietin, *ECM* extracellular matrix, *GRO* growth-regulated oncogene, *IL* interleukin, *MCP-1* monocyte chemoattractant protein-1, *MMP-1* matrix metalloprotease-1, *TIMP* tissue inhibitor of metalloproteinases, *uPAR* urokinase-like plasminogen activator surface receptor

Induction of human endothelial tube formation by exosomes released from 3D-SFnws-adhering HDFs

Finally, we assessed whether the AGFs carried by the exosomes released from 3D-SFnws-adhering HDFs might induce HDMVECs to assemble tubes *in vitro*. Control HDMVECs plated on plastic or ECM gel in 2.5% v/v exosome-depleted FBS medium exhibited only a minimal ability to form tubes (Figure 5a, b). Conversely HDMVECs plated onto ECM gel formed extensive tubular networks in response to the exposure to exosomes released from 3D-SFnws-adhering HDFs (Figure 5c). The conspicuous increases in lengths of the endothelial tubes per microscopic field were alike ($p > 0.05$) for all the tested amounts of added exosomes (Figure 5d). Therefore, the AGFs carried by the exosomes released from 3D-SFnws-adhering HDFs exerted an intense angiogenic activity when contacting HDMVECs *in vitro*.

Discussion

The present carded/hydroentangled 3D-SFnws are scaffolds entirely made of native SF microfibres in β-sheet form isolated from the domesticated silkworm *B. mori*. They represent a technological evolution when compared with the previously reported FA-crosslinked [8] and 3D carded-needled nonwovens [10]. Indeed, both the earlier prototypes performed quite well in terms of biocompatibility and host response following a long-term (up to 6 months) subcutaneous implantation. However, the FA-crosslinked nonwoven was unsatisfactory in terms of biomechanical characteristics. The fact that it remained rather stiff even after an extensive hydration raised serious concerns about its translatability into clinical settings. The second prototype was manufactured according to the carding-needling nonwoven technology, which allowed avoidance of the use of FA as the chemical stabilizer of the scaffold's 3D architecture. In terms of biomechanical

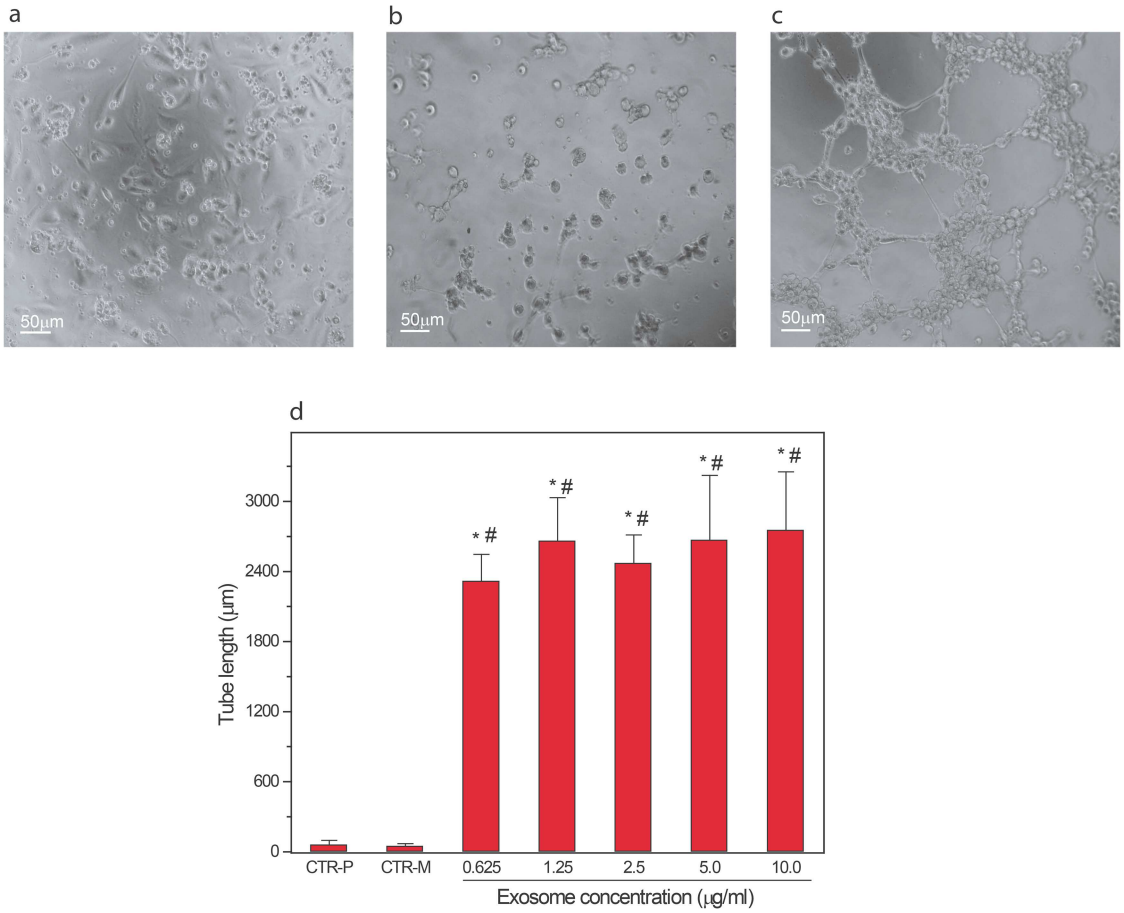

Figure 5. Exosomes released from 3D silk fibroin nonwovens (3D-SFnws)-adhering human dermal fibroblasts (HDFs) induce human dermal microvascular endothelial cells (HDMVECs) to form tubes *in vitro*. **(a)** Micrograph showing plain polystyrene-adhering HDMVECs 5 hours after seeding into a 96-well plate. In each of these wells 20×10^3 HDMVECs were incubated at 37°C in endothelial cell growth basal medium fortified with 2.5% v/v exosome-depleted foetal bovine serum. No HDF-released exosomes were added. **(b)** Micrograph showing HDMVECs 5 hours after seeding onto extracellular matrix (ECM) gel. Save for the latter, the conditions used were the same as in **(a)**. **(c)** Micrograph showing HDMVECs 5 hours after seeding onto ECM gel while being simultaneously exposed to 0.625 μg/ml of exosomes released from 3D-SFnws-adhering HDFs: all the other conditions as in **(a)** and **(b)**. Endothelial tube formation was strongly induced by the HDFs exosomes. **(a–c)** Phase contrast microscopy; original magnification, ×100. **(d)** Bar graph showing the total length (in μm) of newly formed endothelial tubes per microscopic field under the conditions of the test, i.e. (1) control HDMVECs cultured on plain polystyrene (CTR-P) with no addition of exosomes released from 3D-SFnws-adhering HDFs; (2) control HDMVECs cultured on ECM gel (CTR-M) with no addition of exosomes set free from 3D-SFnws-adhering HDFs; and (3) HDMVECs cultured on ECM gel exposed to increasing concentrations of exosomes released from 3D-SFnws-adhering HDFs. Tube formation assay was performed as detailed in the Methods section. The total tube length (in μm)/microscopic field of 332,667 μm^2 area was found via morphometric methods [30] on pictures taken at ×100 magnification of 5 microscopic fields for each exosomal concentration. Triplicate results were averaged and the bars show the means ± standard deviations. As compared to CTR-P or CTR-M, in the total absence of exosomes, the HDMVECs treated with exosomes released from 3D-SFnws-adhering HDFs showed by 5 hours huge increases in the length of endothelial tubes that were dose-independent in the range evaluated. Pairwise one-tailed Student's *t*-test and one-way analysis of variance with *post hoc* Tukey's test were used for statistical analysis. $^{*}p < 0.05$ *vs* CTR-P; $^{\#}p < 0.05$ *vs* CTR-M. Conversely, no statistical difference ($p > 0.05$) in tube length at 5 hours occurred on one hand between CTR-P and CTR-M and on the other hand within the several doses of exosomes evaluated (not shown)

behaviour, the present carded-needled scaffold features were more closely compliant with those of soft biological tissues [10]. However, if on the one hand the use of short length (<25 mm) SF microfibers eased the processing of the raw material with the nonwoven technology, it also led to the production of a very thin (130 μm) sheet that was difficult to handle without its structure becoming misshaping. Regarding the present 3D-SFnws scaffolds, the use of longer SF microfibers (50 mm or a little more) and the shift from nonwoven carding-needling to flat carder-hydroentanglement technology [26] allowed us to produce thicker and mechanically more robust scaffolds. In fact, the 3D-SFnws nonwovens keep all the most appreciable characteristics of the carded-needled prototype (i.e. softness, lightness and interconnected porosity), display an outstanding handling stability (can be safely cut to realize any required size and shape) and provide the opportunity for modulating the biomechanical responses over a wider range of stress and strain values. Moreover, thanks to their mechanical anisotropy, the 3D-SFnws scaffolds are better suited to fulfil the mechanical requirements of soft tissues, such as skin, when subjected to directionally oriented lines of force. All these features make this new 3D-SFnws scaffold a

promising material for the engineered repair and regeneration of soft tissues.

Obtaining an efficient vascularization is one of the crucial problems met when people take aim at engineering/regenerating a body tissue under the guidance of a biomaterial scaffold. An inadequate fulfilment of this target entails serious failures of various degrees. Earlier works from our laboratories showed that the earlier two types of 3D-SFnws implanted into the subcutaneous tissue of C57/BL6 mice were rapidly invaded by newly formed vessels growing first along the SF microfibres and later into the intercalated voids. This intense neoangiogenesis allowed the guided engineering/regeneration of a reticular connective tissue to occur. Between 3 and 6 months later, the newly formed, and by then mature, reticular connective tissue differed from its normal counterpart only by the presence of the SF microfibres and sporadic polynucleated giant cells with no sign at all of fibrosis, encapsulation or thickening of the overlying epidermis [8, 10].

The present results prove, as we hypothesized, that a mechanism based on the release of exosomes carrying significant surpluses of 10 AGFs on the part of 3D-SFnws-adhering HDFs could drive their early vascularization and colonization once grafted to a human tissue *in vivo*. In fact, a tube formation assay showed that the same exosomes powerfully stimulated HDMVECs to produce significant amounts of new tubes, thereby proving their biological pro-angiogenic potential. Previously, Shabbir *et al.* [24] reported that an exposure to exosomes released from mesenchymal stem cells significantly activated protein kinase B/Akt and STAT3 via specific phosphorylations while enhancing the signalling of extracellular-related kinase (ERK)1/2 in normal HDFs. However, further studies will clarify the signalling mechanisms driven by the attachment of the HDFs to 3D-SFnws. Once grafted onto wound sites, the 3D-SFnws will rapidly and effectively promote their own vascularization and cellular colonization through the exosomal release of multiple AGF surpluses from the adhering HDFs (Figure 6). This locally induced neoangiogenesis will increase the SF nonwoven implants success probability, as seen in earlier experiments carried out in rodents *in vivo* [8, 10].

We must mention here studies using different 3D cell culture models *in vitro* releasing exosomes that were more effective in improving angiogenesis and/or functional recovery of various kinds of damaged tissues than those from conventional monolayer (2D) *in vitro* models [18, 36–39]. It is obvious that a 3D environment is more conducive than a 2D one to neoangiogenesis, thereby enhancing skin wound healing [40]. The other hidden advantage of SF-based 3D scaffolds in relation to translational medicine is that humans and other mammals have about 50 if not more proteins that contain significant stretches of conserved amino acid sequences that can be already found in *B. mori*'s SF. This explains the remarkable biocompatibility of the SF-based scaffolds [8, 10, 41].

Finally, the potential biological and applicative impact of each of the AGFs exosomally over-released from 3D-SFnws-adhering HDFs is highlighted in the following paragraphs.

MMP-1, TIMP-1, TIMP-2 and uPAR

According to available data, exosomes carry on their surface discrete amounts of several functionally active proteases, including MMP-1, MMP-2, MMP-3, MMP-9 and MMP-13, ADAM (disintegrin and metallopeptidase domain)-10, ADAM (disintegrin and metallopeptidase domain)-17, hyaluronidase (a glycosidase) and uPAR [42]. The exosomal surface proteases bind and degrade ECM proteins like collagens, laminin and fibronectin. Thus, exosomal proteases modulate the structure of the ECM, thereby creating spaces for newly formed vessels and vessel-associated migrating cells, promoting neoangiogenesis and wound repair.

The present results show that the exosomes released from HDFs cultured on 3D-SFnws carried significantly greater amounts of MMP-1 and its regulatory factor, TIMP-1, than did exosomes freed from HDFs grown on polystyrene. Reportedly, MMP-1 induces angiogenesis by degrading the type I collagen of the ECM and activating the protease-activated receptor-1 [43]. In addition, by blocking the activity of MMP-9, MMP-1 decreases the basal levels of the 24 kDa powerful angiostatic tumstatin, an MMP-9-cleaved fragment of type IV collagen [44, 45]. Of note, the cumulative exosomal contents of MMP-9 did not significantly differ between the 2 experimental groups studied. It is relevant to mention here that an increased expression of both TIMP-1 and TIMP-3 can stabilize the basement membrane and regulate ECM remodelling and angiogenesis at the level of wound beds, thereby promoting epidermal regeneration [46]. Moreover, Lu *et al.* [47] showed that TIMP-1 overexpression activated the phosphoinositide 3-kinase/phospho-Akt pathway, but not the ERK or p38 mitogen-activated protein kinase pathways, thus stimulating the proliferation of mouse NIH-3 T3 fibroblasts in an MMP-independent manner. Conversely, other studies reported that TIMP-1's mitogenic action is MMP-dependent [48].

Our findings show that exosomes released from HDFs cultured on 3D-SFnws carried lesser amounts of TIMP-2 than those from polystyrene-adhering HDFs. TIMP-2 is an endogenous MMP inhibitor which blocks the proliferation of capillary ECs and hence angiogenesis *in vivo* [49]. Interestingly, according to the available evidence, TIMP-2 exerts 2 distinct anti-angiogenic activities: an MMP-dependent one on embryonic neovascularization and an MMP-independent one that inhibits both normal and mitotic factor-driven angiogenesis *in vivo* [49, 50]. Therefore, this decreased exosomal content of TIMP-2 would strengthen the pro-angiogenic actions of other factors carried by the exosomes released from SF-adhering HDFs.

Our present results also revealed that the exosomes from 3D-SFnws-adhering HDFs carried significantly increased

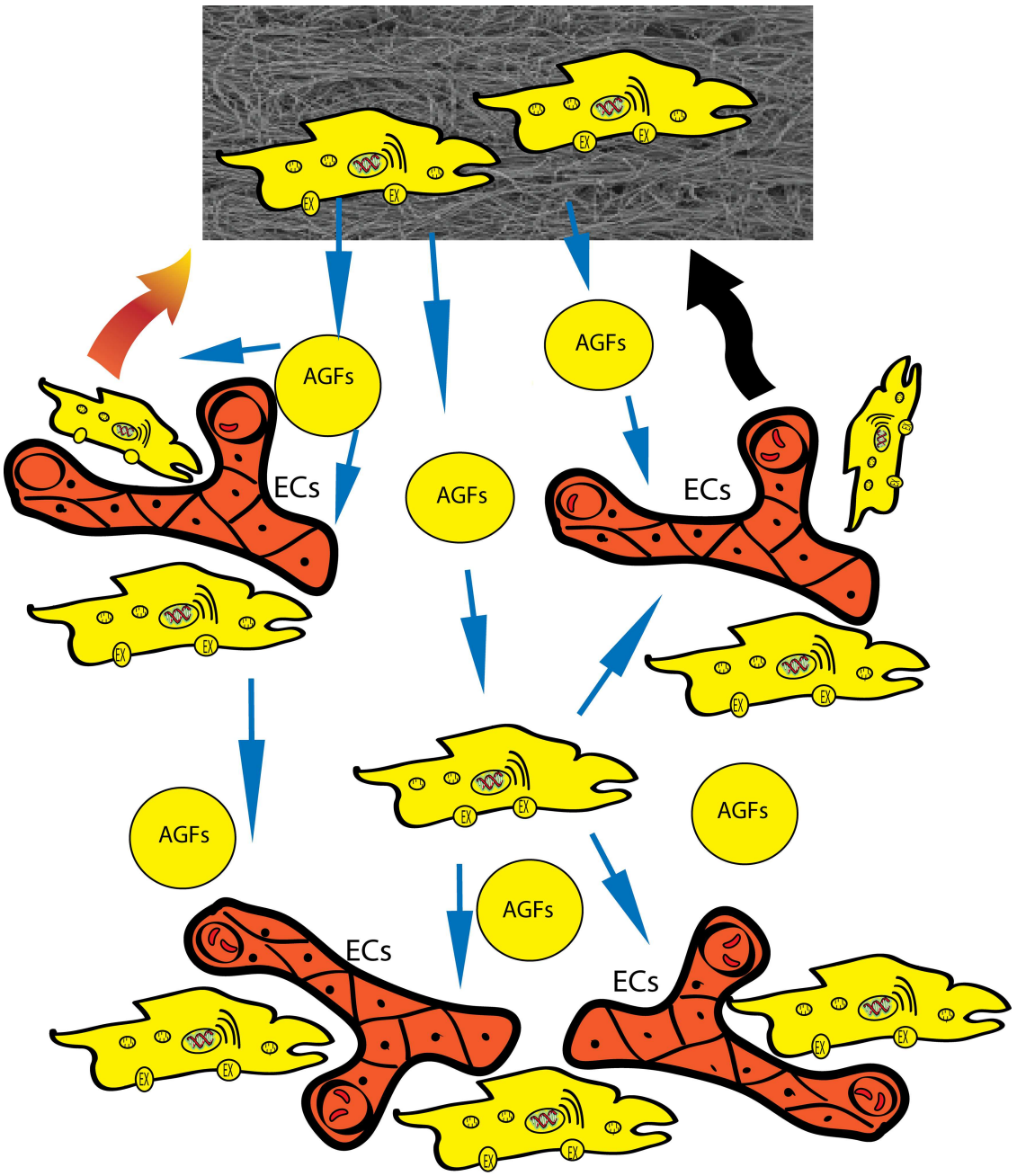

Figure 6. Schematic diagram depicting that human dermal fibroblasts (HDFs) attached to 3D silk fibroin nonwovens (3D-SFnws) (top) release into a wound's connective tissue (bottom) exosomes (EX) carrying surpluses of angiogenic growth factors (AGFs). The transported AGFs are freed onto the external surface of endothelial cells (ECs) of adjoining capillaries and of neighbouring HDFs, thereby activating the proliferation and mobilization of both. The result (not shown but suggested by thick brown-red and black arrows pointing upwards to the 3D-SFnws) is the formation of novel proliferating vessels that invade and colonize the 3D-SFnws graft together with the coming along HDFs. The vascularization and colonization of the SF microfibres and interposed voids end up engineering a new connective tissue differing from the normal one only by the biocompatible SF microfibres [8, 10]

amounts of uPAR, a highly glycosylated, GPI-anchored receptor endowed with 3 extracellular domains (D1–D3). Cleavage between D1 and D2 generates the uPAR D2-D3 fragment, which can be split further [51]. The uPAR ligand, named urokinase-type plasminogen activator (uPA), not only lyses fibrin clots but is also involved in biological processes like angiogenesis, wound healing, embryogenesis, cell migration, inflammation and apoptotic cell death [52]. The onset of angiogenesis critically requires uPA/uPAR-induced ECM degradation [53]. Moreover, uPA/uPAR complexes advance angiogenesis by quelling the expression of their crucial negative regulator, the phosphatase and tensin homolog [54]. Importantly, uPA/uPAR complexes also promote the discharge of various AGFs, like basic FGF/FGF-2 and VEGF, which promote the proliferation of ECs and their ECM invasion [55]. In addition, uPAR complexed with

vitronectin advances adhesion and migration of ECs [56]. The suppression of uPA/uPAR with anti-*uPA* and anti-*uPAR* short hairpin RNAs significantly hindered the pro-angiogenesis signalling by VEGF and granulocyte-macrophage colony-stimulating factor [57, 58]. Finally, soluble full-length uPAR- or uPAR-D2-D3-driven signalling cascades accelerated wound healing via skin epidermal cells, and possibly peri-wound dermal fibroblasts, in K14-Dsg-2 transgenic mice overexpressing desmoglein-2, a crucial component of desmosomes and a regulator of cell survival/proliferation [59].

ANGPT-1, ANGPT-2, (s)Tie-2, and MCP-1/chemokine (C-C motif) ligand-2

The present findings show that exosomes released from HDFs adhering to 3D-SFnws hold significantly higher amounts of ANGPT-1, ANGPT-2 and ANGPT-1-R (or Tie-2) than do those from polystyrene-stuck HDFs. ANGPT-1, ANGPT-2, ANGPT-3 and ANGPT-4 are a group of secreted glycoproteins that bind with similar affinity of the Tie-2 receptors of ECs, activating their tyrosine kinases to phosphorylate their own tyrosine groups. The signalling of ANGPTs/Tie-2/tyrosine kinase complexes crucially regulates venous and lymphatic angiogenesis/remodelling and cardiovascular development [60, 61]. It also protects the vasculature against pathological injuries. On the other hand, the hypoxia-inducible vascular endothelial protein tyrosine phosphatase dephosphorylates and inactivates the Tie-2 receptor [62]. ANGPTs critically mediate reciprocal interactions between ECs and the surrounding ECM. ANGPT-1 promotes the reconstruction and final shape of a mature vascular network endowed with a stable spatial structure [63–66]. ANGPT-1 operates through several mechanisms: (1) it activates the Akt serine kinase, thereby switching on the endothelial nitric oxide synthase 3 [67] and in turn, nitric oxide synthase 3 protects vessels and promotes EC survival; and (2) it raises the phosphorylation of the forkhead box O1 transcription factor, which downregulates the expression of forkhead box O1 target genes [68, 69]. ANGPT-1 overexpression at the skin level significantly improved re-epithelialization and induced a hyper neovascularization. The features of the latter were an increase in vessel numbers coupled with an amplification of vessels size, and the recruitment of endothelial progenitor cells (EPCs) in diabetic wounds. In addition, exogenously administered ANGPT-1 advanced an improved neovascularization which depended on EPC recruitment and exerted beneficial effects on wound re-epithelialization [63]. Moreover, treatment with ANGPT-1 increased the serum levels of pro-MMP-9 and stem cell factor but did not alter VEGF levels [63]. Finally, when co-administered, ANGPT-1 and VEGF enhanced the formation of a collateral circulation [70] and controlled blood vessel growth and permeability [71].

Regarding ANGPT-2, its overexpression increased the Tie-2 receptor phosphorylation promoting the angiogenesis via EC tube formation in renal cell carcinoma (RCC) model mice [72] and the sprouting or regression of vessels in the ovary [66]. Moreover, at high concentrations ANGPT-2 promotes EC survival via the phosphoinositide 3-kinase/Akt signal transduction pathway [73].

A final comment deserves the marginally increased ANGPT-1-R/Tie-2 that occurred in the exosomes released from 3D-SFnws-adhering HDFs. Whether a regulated ectodomain cleavage did release, via exosomes, the soluble ligand-binding domain ((s)Tie-2) of the Tie-2 receptor is an interesting possibility that is still unproven. But let us suppose that it were all in the sTie-2 form: what might it then effect? The work of Alawo *et al.* [74] answers this question. They asked whether increased levels of circulating sTie-2, which occur in cases of myocardial infarction and/or peripheral arteriopathies, might bind ANGPT-1 and supress its actions. Their calculations showed that sTie-2 concentrations effectively suppressing ANGPT-1 signalling must be more than 10-fold higher than those ever detected in healthy or diseased conditions. Therefore, while a local block of ANGPT-1 signalling might occur in cells releasing sTie-2, it is unlikely that the marginal increase in exosomal sTie-2 we observed would hinder ANGPT-1's angiogenic activity.

In our study, the exosomes from HDFs cultured on 3D-SFnws carried significantly lesser amounts of MCP-1 than did those from polystyrene-adhering HDFs. This finding may at least partly explain why the proinflammatory activities of 3D-SFnws are weaker than those of polystyrene. MCP-1, also referred to as chemokine (C-C motif) ligand (CCL)-2, is a small molecule of the chemotactic cytokine family. MCP-1/CCL2 attracts dendritic cells, monocytes and memory T cells to inflammation sites caused by either tissue injury or infection. Fibroblasts, ECs, epithelial cells and leucocytes produce MCP-1/CCL2 during inflammatory processes [75]. A host of CC chemokines, including CCL1, MCP-1/CCL2, CCL3, CCL4, CCL5 and CCL7, are expressed during the first post-injury week in human skin wounds, and elevated levels of MCP-1/CCL2 are detected in human burns [76, 77]. Additionally, the epidermis bordering excisional wounds expresses MCP-1/CCL2 and CCL3 [78]. In healing wounds, gradients of CC chemokine released by hyper-proliferating keratinocytes, fibroblasts and macrophages tightly regulate local phagocytic cell infiltration [79, 80]. The focal adhesion kinase (FAK) is a cytoplasmic protein tyrosine kinase that co-localizes with integrins at sites of attachment to their ligands. Through extracellular signal-regulated kinase (ERK), FAK triggers the secretion of MCP-1 following mechanical stimuli. Fibroblast-specific $FAK^{-/-}$ (knockout) mice exhibited less inflammation and fibrosis than control mice in a hypertrophic scar formation model. Similarly, $MCP\text{-}1^{-/-}$ (knockout) mice formed minimal scars. These findings show that inflammatory chemokine pathways are a major mechanism by which FAK mechano-transduction induces fibrosis [81], a mechanism that *in vivo* grafted 3D-SFnws effectively hindered [8, 10].

IL-1α, IL-4, IL-8/CXCL8, GRO-α GRO-β and GRO-γ

Our present findings show that the exosomes released from 3D-SFnws-adhering HDFs carried higher amounts of IL-1α, IL-4, IL-8/CXCL8, GRO-α, GRO-β and GRO-γ than did those freed from polystyrene-stuck HDFs.

IL-1α and IL-1β belong to the IL-1 cytokine family, whose signalling plays a prominent role in the regulation of angiogenesis and vascular permeability [82]. It is well known that IL-1α can mediate angiogenesis in cancers, the brain and the healing of wounds in which IL-1α and IL-1β act synergistically [83]. IL-1α activates fibroblasts and drives FGF-7 secretion, thus indirectly promoting wound re-epithelization [84]. This stimulation of dermal fibroblasts by IL-1α optimally enhances epidermal stem cell proliferation thereby promoting wound healing and hair regrowth [85].

T helper 2 lymphocytes, mast cells, eosinophils, basophils and (in lesser amounts) fibroblasts typically secrete IL-4, a beneficial anti-inflammatory cytokine. IL-4 hinders the production and secretion of pro-inflammatory cytokines, chemokines, proteases, and reactive oxygen species [86]. Moreover, a controlled release of IL-4 favourably promotes polarization of macrophages from the M1 phenotype, which helps chronicize wounds, to the M2 phenotype, which is beneficial to wound healing [87]. Adding IL-4 to monocytes/macrophages co-cultured with ECs led to a more abundant sprout-like organization of the ECs within the hydrogel [88]. Then again, IL-4 acts both as a proangiogenic and a "fibroblastogenic" cytokine that promotes vessel sprouting, fibroblast proliferation, and fibroblast synthesis of ECM proteins, such as collagen and fibronectin, in normal wound healing [89].

IL-8/CXCL8 is a member of the CXC family and acts as a pro-angiogenic chemokine as it incorporates the Glu-Leu-Arg sequence (the so called ELR motif). The latter allows the formation of IL-8/CXCL8·CXCR2 (C-X-C Motif Chemokine Receptor 2) complexes, thereby inducing a strong angiogenic activity in ECs [90, 91]. The 3 CXCR2 ligands, IL-8/CXCL8, GRO-α and ENA78, have become known as promoters of angiogenesis in tumours [92] and idiopathic pulmonary fibrosis [93, 94]. Together with GRO-α/CXCL1, IL-8/CXCL8 promotes angiogenesis in the sub-epithelial cell layer of the airways [95]. Conversely, IL-8/CXCL8 acts as an anti-angiogenic chemokine when it interacts with the atypical Duffy antigen/chemokine receptor ECs also express [96, 97]. Moreover, by binding the CXCR1 receptor, IL-8/CXCL8 attracts leukocytes to places of inflammation [98]. Besides, metastasis-associated fibroblasts stimulated angiogenesis through the secretion of IL-8/CXCL8 and MCP-1/CCL2 [99]. Interestingly, VEGF and IL-8/CXCL8 co-operated to increase the recruitment of EPCs in skin keloids [100]. Finally, according to mounting evidence, the interaction of adipose-derived stem cells with microvascular ECs promoted angiogenesis by modulating the levels of IL-8/CXCL8, IL-6, MCP-1 and VEGF, thus advancing the healing of chronic soft tissue wounds [101].

Human chemokines GRO-α/CXCL1, GRO-β/CXCL2 and GRO-γ/CXCL3 are products of 3 distinct, non-allelic genes. GRO-β and GRO-γ share a 90% and 86% amino acid sequence homology, respectively, with GRO-α. They are members of the CXC family endowed with an ELR motif and, when they interact with the CXCR2 receptor, promote EC proliferation and migration, angiogenesis and neovascularization even in the absence of a concurrent tissue inflammation [91]. Normal human epidermis expresses GRO-α/CXCL1 and GRO-β/CXCR2, which are especially involved in the healing of human burn wounds [102]. GRO-α/CXCL1 attracts neutrophils, is upregulated in acute wounds and, by promoting keratinocyte migration, advances wound reepithelization [76, 103]. In addition, GRO-α/CXCL1 is one of the chemokines endowed with liver regenerative powers [104] and, as just mentioned, acting together with IL-8/CXCL8, promotes angiogenesis in the sub-epithelial cell layer of airways [95] and in cases of Sjögren's syndrome [105]. Heightened, as compared to controls, serum levels of GRO-α/CXCL1 were taken as markers of angiogenesis and inflammation in patients with type 2 diabetes [106]. GRO-β/CXCL2 chemokine is of importance for the correct breaching of EC junctions [107]. Finally, scleroderma microvascular ECs are unresponsive to GRO-γ/CXCL3·CXCR2 signalling [108].

Conclusions

The present results show that HDFs grown on a novel kind of 3D-SFnws release exosomes that hold significant amounts of several cytokines, chemokines and other factors, some of which mainly advance angiogenesis (i.e. ANGPT-1, ANGPT-2, Tie-2), some both angiogenesis and mitogenesis (i.e. IL-1α, IL-4, IL-8, GRO-α, GRO-β and GRO-γ) and a few of which are more involved in ECM's proangiogenic remodelling (i.e. MMP-1, TIMP-1, uPAR). The amounts of said factors were significantly higher in the exosomes released from 3D-SFnws-adhering HDFs than in those released from polystyrene-stuck monolayered HDFs. These results suggest that the exosomal over-release of angiogenic and trophic factors from the SF-adhering HDFs did promote, once grafted into the skin subcutaneous tissue of living mice, the early-onset, quick and abundant vascularization and cellular colonization of the previously studied 2 types of 3D-SFnws. The same results prove that the exosomes released from 3D-SFnws-adhering HDFs exert a powerful proangiogenic stimulus on HDMVECs. These crucial consequences of the interactions between SF microfibers and non-tumorigenic HDFs and HDMVECs are well worth further studies related to the application of 3D SF-based nonwoven grafts in human (and even veterinary) clinical settings for the guided engineering, neovascularization and regeneration of substantial skin losses due to burns, diabetic ulcers, traumata or other kinds of wounding agents.

Supplementary data

Supplementary data is available at *Burns & Trauma Journal* online.

Authors' contributions

All authors contributed to the design of the study, performance of the experiments and the writing of the manuscript. GF and UA conceived and produced the novel 3D silk fibroin nonwovens. GF characterized the 3D silk fibroin nonwovens. PH, AC and IDP conceived and performed the *in vitro* cellular and biochemical experiments. PH, AC and IDP also collected the results under the supervision of UA. JW and KN statistically analysed the results and critically edited the manuscript. All authors read and agreed to publish this version of the manuscript.

Funding

The FUR 2018 of the Ministry of Italian University and Research funded this research work. No further funding from private or commercial sources supported it. PH holds a triannual doctorate student fellowship from the INVITE project funded by the European Union's Horizon 2020 Research and Innovation Program under the Marie Sklodowska-Curie Grant Agreement No. 754345.

Availability of data and materials

The datasets of this study are available upon request to the corresponding authors.

Conflicts of interest

The authors IDP, AC, JW, UA, KN and HP declare no conflict of interest. GF is co-founder and shareholder of Silk Biomaterials S.r.l.

Abbreviations

3D-SFnws: 3D silk fibroin nonwovens; AGFs: angiogenic/growth factors; Akt: protein kinase B or PKB; ANGPT: angiopoietin; CCL: chemokine (C-C motif) ligand; CXCL8: chemokine (C-X-C motif) ligand 8; CXCR2: (C-X-C Motif Chemokine Receptor 2); ECM: extracellular matrix; ECs: endothelial cells; ELISA: enzyme-linked immunosorbent assay; EPCs: endothelial progenitor cells; ERK: extracellular-signal-regulated kinase; FA: formic acid; FAK: focal adhesion kinase; FBS: foetal bovine serum; FGF: fibroblast growth factor; GRO: growth-regulated oncogene; HDFs: human dermal fibroblasts; HDMVECs: human dermal microvascular endothelial cells; IL: interleukin; MCP-1: monocyte chemoattractant protein-1; MD: machine direction; MMP: matrix metalloprotease; SDs: standard deviations; SF: silk fibroin; TD: transversal direction; TIMP: tissue inhibitor of metalloproteinase; uPA: urokinase-like plasminogen activator; uPAR: urokinase-type plasminogen activator surface receptor; VEGF: vascular endothelial growth factor.

Acknowledgements

The authors thank Professors Pier Francesco Nocini, Verona University Dean, and Giovanni De Manzoni, Head of the Department of Surgery, Dentistry, Paediatrics and Gynaecology, of the Medical School, University of Verona, for their support.

References

1. Guo C, Zhang J, Jordan JS, Wang X, Henning RW, Yarger JL. Structural comparison of various silkworm silks: an insight into the structure-property relationship. *Biomacromolecules*. 2018;19:906–17.
2. Altman GH, Diaz F, Jakuba C, Calabro T, Horan RL, Chen J, *et al*. Silk-based biomaterials. *Biomaterials*. 2003;24:401–16.
3. Thurber AE, Omenetto FG, Kaplan DL. In vivo bioresponses to silk proteins. *Biomaterials*. 2015;71:145–57.
4. Rockwood DN, Preda RC, Yücel T, Wang X, Lovett ML, Kaplan DL. Materials fabrication from Bombyx mori silk fibroin. *Nat Protoc*. 2011;6:1612–31.
5. Li C, Guo C, Fitzpatrick V, Ibrahim A, Zwierstra MJ, Hanna P, *et al*. Design of biodegradable, implantable devices towards clinical translation. *Nat Rev Mat*. 2020;5:61–81.
6. Holland C, Numata K, Rnjak-Kovacina J, Seib FP. The biomedical use of silk: past, present, future. *Adv Healthc Mater*. 2019. https://doi.org/10.1002/adhm.201800465.
7. Edana, the voice of nonwovens. At: https://www.edana.org/docs/default-source/edana-nonwovens/iso-and-cen-definition-of-nonwovens.pdf?sfvrsn=21822973_221.
8. Dal Prà I, Freddi G, Minic J, Chiarini A, Armato U. De novo engineering of reticular connective tissue in vivo by silk fibroin nonwoven materials. *Biomaterials*. 2005;26:1987–99.
9. Dal Prà I, Chiarini A, Boschi A, Freddi G, Armato U. Novel dermo-epidermal equivalents on silk fibroin-based formic acid-crosslinked three-dimensional nonwoven devices with prospective applications in human tissue engineering/regeneration/repair. *Int J Mol Med*. 2006;18:241–7.
10. Chiarini A, Freddi G, Liu D, Armato U, Dal Prà I. Biocompatible silk noil-based three-dimensional carded-needled nonwoven scaffolds guide the engineering o novel skin connective tissue. *Tissue Eng Part A*. 2016;22:1047–60.
11. Smith RS, Smith TJ, Blieden TM, Phipps RP. Fibroblasts as sentinel cells. Synthesis of chemokines and regulation of inflammation. *Am J Pathol*. 1997;151:317–22.
12. Witowski J, Thiel A, Dechend R, Dunkel K, Fouquet N, Bender TO, *et al*. Synthesis of C-X-C and C-C chemokines by human peritoneal fibroblasts: induction by macrophage-derived cytokines. *Am J Pathol*. 2001;158:1441–50.
13. Bang C, Thum T. Exosomes: new players in cell-cell communication. *Int J Biochem Cell Biol*. 2012;44:2060–4.
14. Grimstad Ø, Sandanger Ø, Ryan L, Otterdal K, Damaas JK, Pukstad B, *et al*. Cellular sources and inducers of cytokines present in acute wound fluid. *Wound Repair Regen* 2011;19:337–47.
15. Cvikl B, Lussi A, Moritz A, Sawada K, Gruber R. Differential inflammatory response of dental pulp explants and fibroblasts to saliva. *Int Endod J*. 2016;49:655–62.
16. Ohta K, Naruse T, Kato H, Ishida Y, Nakagawa T, Ono S, *et al*. Differential regulation by IFN-γ on TNF-α-induced chemokine expression in synovial fibroblasts from temporomandibular joint. *Mol Med Rep*. 2017;16:6850–7.

17. Tokarz A, Szuścik I, Kuśnierz-Cabala B, Kapusta M, Konkolewska M, Żurakowski A, *et al.* Extracellular vesicles participate in the transport of cytokines and angiogenic factors in diabetic patients with ocular complications. *Folia Med Cracov.* 2015;55:35–48.
18. Yan L, Wu X, Wu X. Exosomes produced from 3D cultures of umbilical cord mesenchymal stem cells in a hollow-fiber bioreactor show improved osteochondral regeneration activity. *Cell Biol Toxicol.* 2020;36:165–78.
19. Hu S, Li Z, Cores J, Huang K, Su T, Dinh PU, *et al.* Needle-free injection of exosomes derived from human dermal fibroblast spheroids ameliorates skin Photoaging. *ACS Nano.* 2019;13:11273–82.
20. Fitzgerald W, Freeman ML, Lederman MM, Vasilieva E, Romero R, Margolis L. A system of cytokines encapsulated in extracellular vesicles. *Sci Rep.* 2018. https://doi.org/10.1038/s41598-018-27190-x.
21. Gurunathan S, Kang MH, Jeyaraj M, Qasim M, Kim JH. Review of the isolation, characterization, biological function, and multifarious therapeutic approaches of exosomes. *Cell.* 2019. https://doi.org/10.3390/cells8040307.
22. Hu P, Yang Q, Wang Q, Shi C, Wang D, Armato U, *et al.* Mesenchymal stromal cells-exosomes: a promising cell-free therapeutic tool for wound healing and cutaneous regeneration. *Burns Trauma.* 2019. https://doi.org/10.1186/s41038-019-0178-8.
23. Barnes BJ, Somerville CC. Modulating cytokine production via select packaging and secretion from extracellular vesicles. *Front Immunol.* 2020. https://doi.org/10.3389/fimmu.2020.01040.
24. Shabbir A, Cox A, Rodriguez-Menocal L, Salgado M, Van Badiavas E. Mesenchymal stem cell exosomes induce proliferation and migration of normal and chronic wound fibroblasts, and enhance angiogenesis in vitro. *Stem Cells. Dev* 2015; 24: 1635–47.
25. Baruah J, Wary KK. Exosomes in the regulation of vascular endothelial cell regeneration. *Front Cell Dev Biol.* 2020. https://doi.org/10.3389/fcell.2019.00353.
26. Edwards JV, Graves E, Prevost N, Condon B, Yager D, Dacorta J, *et al.* Development of a nonwoven hemostatic dressing based on unbleached cotton: a de novo design approach. *Pharmaceutics.* 2020. https://doi.org/10.3390/pharmaceutics12070609.
27. Chiarini A, Armato U, Gardenal E, Gui L, Dal Prà I. Amyloid β-exposed human astrocytes overproduce Phospho-tau and Overrelease it within exosomes, effects suppressed by Calcilytic NPS 2143-further implications for Alzheimer's therapy. *Front Neurosci.* 2017. https://doi.org/10.3389/fnins.2017.00217.
28. Patel GK, Khan MA, Zubair H, Srivastava SK, Khushman M, Singh S, *et al.* Comparative analysis of exosome isolation methods using culture supernatant for optimum yield, purity and downstream applications. *Sci Rep.* 2019. https://doi.org/10.1038/s41598-019-41800-2.
29. Nakamura K, Jinnin M, Harada M, Kudo H, Nakayama W, Inoue K, *et al.* Altered expression of CD63 and exosomes in scleroderma dermal fibroblasts. *J Dermatol Sci.* 2016;84: 30–9.
30. Armato U, Romano F, Andreis PG, Paccagnella L, Marchesini C. Growth stimulation and apoptosis induced in cultures of neonatal rat liver cells by repeated exposures to epidermal growth factor/urogastrone with or without associated pancreatic hormones. *Cell Tissue Res.* 1986;245:471–80.
31. Zhang K, Mo X, Huang C, He C, Wang H. Electrospun scaffolds from silk fibroin and their cellular compatibility. *J Biomed Mater Res A.* 2010;93:976–983.
32. Lotz B, Colonna Cesari F. The chemical structure and the crystalline structures of Bombyx mori silk fibroin. *Biochimie.* 1979;61:205.
33. Holzapfel GA. Biomechanics of soft tissue in. In: Lemaitre J (ed). *Handbook of Materials Behavior Models*. Burlington: Academic Press, 2001, 1057–71.
34. Wang Y, Rudym DD, Walsh A, Abrahamsen L, Kim HJ, Kim HS, *et al.* In vivo degradation of three-dimensional silk fibroin scaffolds. *Biomaterials.* 2008;29:3415–28.
35. Huang R, Jiang W, Yang J, Mao YQ, Zhang Y, Yang W, *et al.* A biotin label-based antibody array for high-content profiling of protein expression. *Cancer Genomics Proteomics.* 2010;7:129–41.
36. Zhang Y, Chopp M, Zhang ZG, Katakowski M, Xin H, Qu C, *et al.* Systemic administration of cell-free exosomes generated by human bone marrow derived mesenchymal stem cells cultured under 2D and 3D conditions improves functional recovery in rats after traumatic brain injury. *Neurochem Int.* 2017;111:69–81.
37. Sun Y, Wang Y, Zhou L, Zou Y, Huang G, Gao G, *et al.* Spheroid-cultured human umbilical cord-derived mesenchymal stem cells attenuate hepatic ischemia-reperfusion injury in rats. *Sci Rep.* 2018. https://doi.org/10.1038/s41598-018-20975-0.
38. Kim MH, Wu WH, Choi JH, Kim J, Jun JH, Ko Y, *et al.* Galectin-1 from conditioned medium of three-dimensional culture of adipose-derived stem cells accelerates migration and proliferation of human keratinocytes and fibroblasts. *Wound Repair Regen.* 2018;26 Suppl 1:S9–18.
39. Martin M, Veloso A, Wu J, Katrukha EA, Akhmanova A. Control of endothelial cell polarity and sprouting angiogenesis by non-centrosomal microtubules. *Elife.* 2018. https://doi.org/10.7554/eLife.33864.
40. Du P, Suhaeri M, Ha SS, Oh SJ, Kim SH, Park K. Human lung fibroblast-derived matrix facilitates vascular morphogenesis in 3D environment and enhances skin wound healing. *Acta Biomater.* 2017;54:333–44.
41. Armato U, Dal Pra I, Chiarini A. Freddi. Will silk fibroin nanofiber scaffolds ever hold a useful place in translational regenerative medicine? *Int J Burns Trauma.* 2011;1:27–33.
42. Mu W, Rana S, Zöller M. Host matrix modulation by tumor exosomes promotes motility and invasiveness. *Neoplasia.* 2013;15:875–87.
43. Zheng J, Fan H, Chen Y, Ni B, Wang S, Sun M, *et al.* Expression of MMP-1/PAR-1 and patterns of invasion in oral squamous cell carcinoma as potential prognostic markers. *Onco Targets Ther.* 2015;8:1619–26.
44. Liu H, Chen B, Lilly B. Fibroblasts potentiate blood vessel formation partially through secreted factor TIMP-1. *Angiogenesis.* 2008;11:223–34.
45. Mauldin GN, Foster TP, Waddell CW, Egan ME. Cloning, expression and in vitro evaluation of recombinant canine Tum5, an angiostatic domain of mammalian type IV collagen. *Vet Comp Oncol.* 2003;1:36–47.
46. Vaalamo M, Leivo T, Saarialho-Kere U. Differential expression of tissue inhibitors of metalloproteinases (TIMP-1, −2, −3, and −4) in normal and aberrant wound healing. *Hum Pathol.* 1999;30:795–802.

47. Lu Y, Liu S, Zhang S, Cai G, Jiang H, Su H, *et al.* Tissue inhibitor of metalloproteinase-1 promotes NIH3T3 fibroblast proliferation by activating p-Akt and cell cycle progression. *Mol Cells*. 2011;31:225–30.
48. Porter KE, Turner NA, O'Regan DJ, Ball SG. Tumor necrosis factor alpha induces human atrial myofibroblast proliferation, invasion and MMP-9 secretion: inhibition by simvastatin. *Cardiovasc Res*. 2004;64:507–15.
49. Fernández CA, Butterfield C, Jackson G, Moses MA. Structural and functional uncoupling of the enzymatic and angiogenic inhibitory activities of tissue inhibitor of metalloproteinase-2 (TIMP-2): loop 6 is a novel angiogenesis inhibitor. *J Biol Chem*. 2003;278:40989–95.
50. Stetler-Stevenson WG, Seo DW. TIMP-2: an endogenous inhibitor of angiogenesis. *Trends Mol Med*. 2005;11:97–103.
51. Sidenius N, Sier CF, Blasi F. Shedding and cleavage of the urokinase receptor (uPAR): identification and characterisation of uPAR fragments in vitro and in vivo. *FEBS Lett*. 2000;475:52–6.
52. McMahon BJ, Kwaan HC. Components of the plasminogen-plasmin system as biologic markers for cancer. *Adv Exp Med Biol*. 2015;867:145–56.
53. Su S-C, Lin C-W, Yang W-E, Fan W-L, Yang S-F. The urokinase-type plasminogen activator (uPA) system as a biomarker and therapeutic target in human malignancies. *Expert Opin Ther Targets*. 2016;20:551–66.
54. Unseld M, Chilla A, Pausz C, Mawas R, Breuss J, Zielinski C, *et al.* PTEN expression in endothelial cells is down-regulated by uPAR to promote angiogenesis. *Thromb Haemost*. 2015;114:379–89.
55. Gerwins P, Sköldenberg E, Claesson-Welsh L. Function of fibroblast growth factors and vascular endothelial growth factors and their receptors in angiogenesis. *Crit Rev Oncol Hematol*. 2000;34:185–94.
56. Preissner KT, Reuning U. Vitronectin in vascular context: facets of a multitalented matricellular protein. *Semin Thromb Hemost*. 2011;37:408–24.
57. Gondi CS, Lakka SS, Dinh DH, Olivero WC, Gujrati M, Rao JS. Intraperitoneal injection of a hairpin RNA–expressing plasmid targeting urokinase-type plasminogen activator (uPA) receptor and uPA retards angiogenesis and inhibits intracranial tumor growth in nude mice. *Clin Cancer Res*. 2007;13:4051–60.
58. Raghu H, Nalla AK, Gondi CS, Gujrati M, Dinh DH. Rao JS. uPA and uPAR shRNA inhibit angiogenesis via enhanced secretion of SVEGFR1 independent of GM-CSF but dependent on TIMP-1 in endothelial and glioblastoma cells. *Mol Oncol*. 2012;6:33–47.
59. Cooper F, Overmiller AM, Loder A, Brennan-Crispi DM, McGuinn KP, Marous MR, *et al.* Enhancement of cutaneous wound healing by Dsg2 augmentation of uPAR secretion. *J Invest Dermatol*. 2018;138:2470–9.
60. Augustin HG, Koh G-Y. Organotypic vasculature: from descriptive heterogeneity to functional pathophysiology. *Science*. 2017. https://doi.org/10.1126/science.aal2379.
61. Saharinen P, Leppänen VM, Alitalo K. Snapshot: angiopoietins and their functions. *Cell*. 2017;171:724–4.
62. Frye M, Dierkes M, Küppers V, Vockel M, Tomm J, Zeuschner D, *et al.* Interfering with VE-PTP stabilizes endothelial junctions in vivo via Tie-2 in the absence of VE-cadherin. *J Exp Med*. 2015;212:2267–87.
63. Balaji S, Han N, Moles C, Shaaban AF, Bollyky PL, Crombleholme TM, *et al.* Angiopoietin-1 improves endothelial progenitor cell-dependent neovascularization in diabetic wounds. *Surgery*. 2015;158:846–56.
64. Kim I, Kim HG, Moon SO, Chae SW, So JN, Koh KN, *et al.* Angiopoietin-1 induces endothelial cell sprouting through the activation of focal adhesion kinase and plasmin secretion. *Circ Res*. 2000;86:952–9.
65. Kim I, Kim HG, So JN, Kim JH, Kwak HJ, Koh GY. Angiopoietin-1 regulates endothelial cell survival through the phosphatidylinositol 3′-kinase/Akt signal transduction pathway. *Circ Res*. 2000;86:24–9.
66. Yancopoulos GD, Davis S, Gale NW, Rudge JS, Wiegand SJ, Holash J. Vascular-specific growth factors and blood vessel formation. *Nature*. 2000;407:242–8.
67. Babaei S, Teichert-Kuliszewska K, Zhang Q, Jones N, Dumont DJ, Stewart DJ. Angiogenic actions of angiopoietin-1 require endothelium-derived nitric oxide. *Am J Pathol*. 2003;162:1927–36.
68. Kim JH, Shin JP, Kim IT, Park DH. Aqueous angiopoietin-like 4 levels correlate with nonperfusion area and macular edema in branch retinal vein occlusion. *Invest Ophthalmol Vis Sci*. 2016;57:6–11.
69. Korhonen EA, Lampinen A, Giri H, Anisimov A, Kim M, Allen B, *et al.* Tie1 controls angiopoietin function in vascular remodeling and inflammation. *J Clin Invest*. 2016;126:3495–510.
70. Chae JK, Kim I, Lim ST, Chung MJ, Kim WH, Kim HG, *et al.* Coadministration of angiopoietin-1 and vascular endothelial growth factor enhances collateral vascularization. *Arterioscler Thromb Vasc Biol*. 2000;20:2573–8.
71. Thurston G. Complementary actions of VEGF and angiopoietin-1 on blood vessel growth and leakage. *J Anat*. 2002;200:575–80.
72. Gu J, Zhang Y, Han Z, Gao L, Cui J, Sun Y, *et al.* Targeting the ERβ/Angiopoietin-2/Tie-2 signaling-mediated angiogenesis with the FDA-approved anti-estrogen Faslodex to increase the Sunitinib sensitivity in RCC. *Cell Death Dis*. 2020;11:367.
73. Kim I, Kim JH, Moon SO, Kwak HJ, Kim NG, Koh GY. Angiopoietin-2 at high concentration can enhance endothelial cell survival through the phosphatidylinositol 3′-kinase/Akt signal transduction pathway. *Oncogene*. 2000;19:4549–52.
74. Alawo DOA, Tahir TA, Fischer M, Bates DG, Amirova SR, Brindle NPJ. Regulation of angiopoietin signalling by soluble Tie2 ectodomain and engineered ligand trap. *Sci Rep*. 2017. https://doi.org/10.1038/s41598-017-03981-6.
75. Sanchez B, Li L, Dulong J, Aimond G, Lamartine J, Liu G, *et al.* Impact of human dermal microvascular endothelial cells on primary dermal fibroblasts in response to inflammatory stress. *Front Cell Dev Biol*. 2019. https://doi.org/10.3389/fcell.2019.00044.
76. Engelhardt E, Toksoy A, Goebeler M, Debus S, Bröcker EB, Gillitzer R. Chemokines IL-8, GRO alpha, MCP-1, IP-10, and Mig are sequentially and differentially expressed during phase-specific infiltration of leukocyte subsets in human wound healing. *Am J Pathol*. 1998;153:1849–60.
77. Gibran NS, Ferguson M, Heimbach DM, Isik FF. Monocyte chemoattractant protein-1 mRNA expression in the human burn wound. *J Surg Res*. 1997;70:1–6.
78. Jackman SH, Yoak MB, Keerthy S, Beaver BL. Differential expression of chemokines in a mouse model of wound healing. *Ann Clin Lab Sci*. 2000;30:201–7.

79. Eming SA, Krieg T, Davidson JM. Inflammation in wound repair: molecular and cellular mechanisms. *J Investig Dermatol*. 2007;127:514–25.
80. Gillitzer R, Goebeler M. Chemokines in cutaneous wound healing. *J Leukoc Biol*. 2001;69:513–21.
81. Wong VW, Rustad KC, Akaishi S, Sorkin M, Glotzbach JP, Januszyk M, *et al*. Focal adhesion kinase links mechanical force to skin fibrosis via inflammatory signaling. *Nat Med*. 2011;18:148–52.
82. Fahey E, Doyle SLIL. 1 family cytokine regulation of vascular permeability and angiogenesis. *Front Immunol*. 2019;10:1426.
83. Salmeron K, Aihara T, Redondo-Castro E, Pinteaux E, Bix G. IL-1alpha induces angiogenesis in brain endothelial cells in vitro: implications for brain angiogenesis after acute injury. *J Neurochem*. 2016;136:573–80.
84. Tang A, Gilchrest BA. Regulation of keratinocyte growth factor gene expression in human skin fibroblasts. *J Dermatol Sci*. 1996;11:41–50.
85. Lee P, Gund R, Dutta A, Pincha N, Rana I, Ghosh S, *et al*. Stimulation of hair follicle stem cell proliferation through an IL-1 dependent activation of $\gamma\delta$T-cells. *Elife*. 2017. https://doi.org/10.7554/eLife.28875.
86. Wills-Karp M, Finkelman FD. Untangling the complex web of IL-4- and IL-13-mediated signaling pathways. *Sci Signal*. 2008. https://doi.org/10.1126/scisignal.1.51.pe55.
87. Li M, Gao L, Chen J, Zhang Y, Wang J, Lu X, *et al*. Controllable release of interleukin-4 in double-layer sol-gel coatings on TiO_2 nanotubes for modulating macrophage polarization. *Biomed Mater*. 2018. https://doi.org/10.1088/1748-605X/aa9526.
88. Barthes J, Dollinger C, Muller CB, Liivas U, Dupret-Bories A, Knopf-Marques H, *et al*. Immune assisted tissue engineering via incorporation of macrophages in cell-laden hydrogels under cytokine stimulation. *Front Bioeng Biotechnol*. 2018. https://doi.org/10.3389/fbioe.2018.00108.
89. Postlethwaite AE, Holness MA, Katai H, Raghow R. Human fibroblasts synthesize elevated levels of extracellular matrix proteins in response to interleukin 4. *J Clin Invest*. 1992;90:1479–85.
90. Koch AE, Polverini PJ, Kunkel SL, Harlow LA, DiPietro L, Elner VM, *et al*. Interleukin-8 as a macrophage-derived mediator of angiogenesis. *Science*. 1992;258:1798–801.
91. Strieter RM, Polverini PJ, Kunkel SL, Arenberg DA, Burdick MD, Kasper J, *et al*. The functional role of the ELR motif in CXC chemokine- mediated angiogenesis. *J Biol Chem*. 1995;270:27348–57.
92. Strieter RM, Burdick MD, Mestas J, Gomperts B, Keane MP, Belperio JA. Cancer CXC chemokine networks and tumour angiogenesis. *Eur J Cancer*. 2006;42:768–78.
93. Keane MP, Arenberg DA, Lynch JP, III, Whyte RI, Iannettoni MD, Burdick MD, *et al*. The CXC chemokines, IL-8 and IP-10, regulate angiogenic activity in idiopathic pulmonary fibrosis. *J Immunol*. 1997;159:1437–43.
94. Keane MP, Belperio JA, Burdick MD, Lynch JP, III, Fishbein MC, Strieter RM. ENA-78 is an important angiogenic factor in idiopathic pulmonary fibrosis. *Am J Respir Crit Care Med*. 2001;164:2239–42.
95. Keglowich L, Roth M, Philippova M, Resink T, Tjin G, Oliver B, *et al*. Bronchial smooth muscle cells of asthmatics promote angiogenesis through elevated secretion of CXC-chemokines (ENA-78, GRO-α, and IL-8). *PLoS One*. 2013. https://doi.org/10.1371/journal.pone.0081494.
96. Dawson TC, Lentsch AB, Wang Z, Cowhig JE, Rot A, Maeda N, *et al*. Exaggerated response to endotoxin in mice lacking the Duffy antigen/re- ceptor for chemokines (DARC). *Blood*. 2000;96:1681–4.
97. Horton LW, Yu Y, Zaja-Milatovic S, Strieter RM, Richmond A. Opposing roles of murine duffy antigen receptor for chemokine and murine CXC chemokine receptor-2 receptors in murine melanoma tumor growth. *Cancer Res*. 2007;67:9791–9.
98. Ramjeesingh R, Leung R, Siu CH. Interleukin-8 secreted by endothelial cells induces chemotaxis of melanoma cells through the chemokine receptor CXCR1. *FASEB J*. 2003;17:1292–4.
99. Pausch TM, Aue E, Wirsik NM, Freire Valls A, Shen Y, Radhakrishnan P, *et al*. Metastasis-associated fibroblasts promote angiogenesis in metastasized pancreatic cancer via the CXCL8 and the CCL2 axes. *Sci Rep*. 2020. https://doi.org/10.1038/s41598-020-62416-x.
100. Tanaka R, Umeyama Y, Hagiwara H, Ito-Hirano R, Fujimura S, Mizuno H, *et al*. Keloid patients have higher peripheral blood endothelial progenitor cell counts and $CD34^+$ cells with normal vasculogenic and angiogenic function that overexpress vascular endothelial growth factor and interleukin-8. *Int J Dermatol*. 2019;58:1398–405.
101. Bachmann S, Jennewein M, Bubel M, Guthörl S, Pohlemann T, Oberringer M. Interacting adipose-derived stem cells and microvascular endothelial cells provide a beneficial milieu for soft tissue healing. *Mol Biol Rep*. 2020;47:111–22.
102. Zaja-Milatovic S, Richmond A. CXC chemokines and their receptors: a case for a significant biological role in cutaneous wound healing. *Histol Histopathol*. 2008;23:1399–407.
103. Christopherson K III, Hromas R. Chemokine regulation of normal and pathologic immune responses. *Stem Cells*. 2001;19:388–96.
104. Chinnici CM, Pietrosi G, Iannolo G, Amico G, Cuscino N, Pagano V, *et al*. Mesenchymal stromal cells isolated from human fetal liver release soluble factors with a potential role in liver tissue repair. *Differentiation*. 2019;105:14–26.
105. Lisi S, Sisto M, Lofrumento DD, D'Amore M, De Lucro R, Ribatti D. A potential role of the GRO-α/CXCR2 system in Sjögren's syndrome: regulatory effects of pro-inflammatory cytokines. *Histochem Cell Biol*. 2013;139:371–9.
106. Sajadi SM, Khoramdelazad H, Hassanshahi G, Rafatpanah H, Hosseini J, Mahmoodi M, *et al*. Plasma levels of CXCL1 (GRO-alpha) and CXCL10 (IP-10) are elevated in type 2 diabetic patients: evidence for the involvement of inflammation and angiogenesis/angiostasis in this disease state. *Clin Lab*. 2013;59:133–7.
107. Girbl T, Lenn T, Perez L, Rolas L, Barkaway A, Thiriot A, *et al*. Distinct compartmentalization of the chemokines CXCL1 and CXCL2 and the atypical receptor ACKR1 determine discrete stages of neutrophil diapedesis. *Immunity*. 2018;49:1062, e6–76.
108. Tsou PS, Rabquer BJ, Ohara RA, Stinson WA, Campbell PL, Amin MA, *et al*. Scleroderma dermal microvascular endothelial cells exhibit defective response to pro-angiogenic chemokines. *Rheumatology (Oxford)*. 2016;55:745–54.